AD-A057 281 ROME AIR DEVELOPMENT CENTER GRIFFISS AFB N Y F/G 9/5
A UHF/EHF HYBRID ANTENNA,(U)
MAR 78 J A STROM, R J MAILLOUX, L F DENNETT
UNCLASSIFIED RADC-TR-78-79 NL

1 OF 1
AD
A057 281

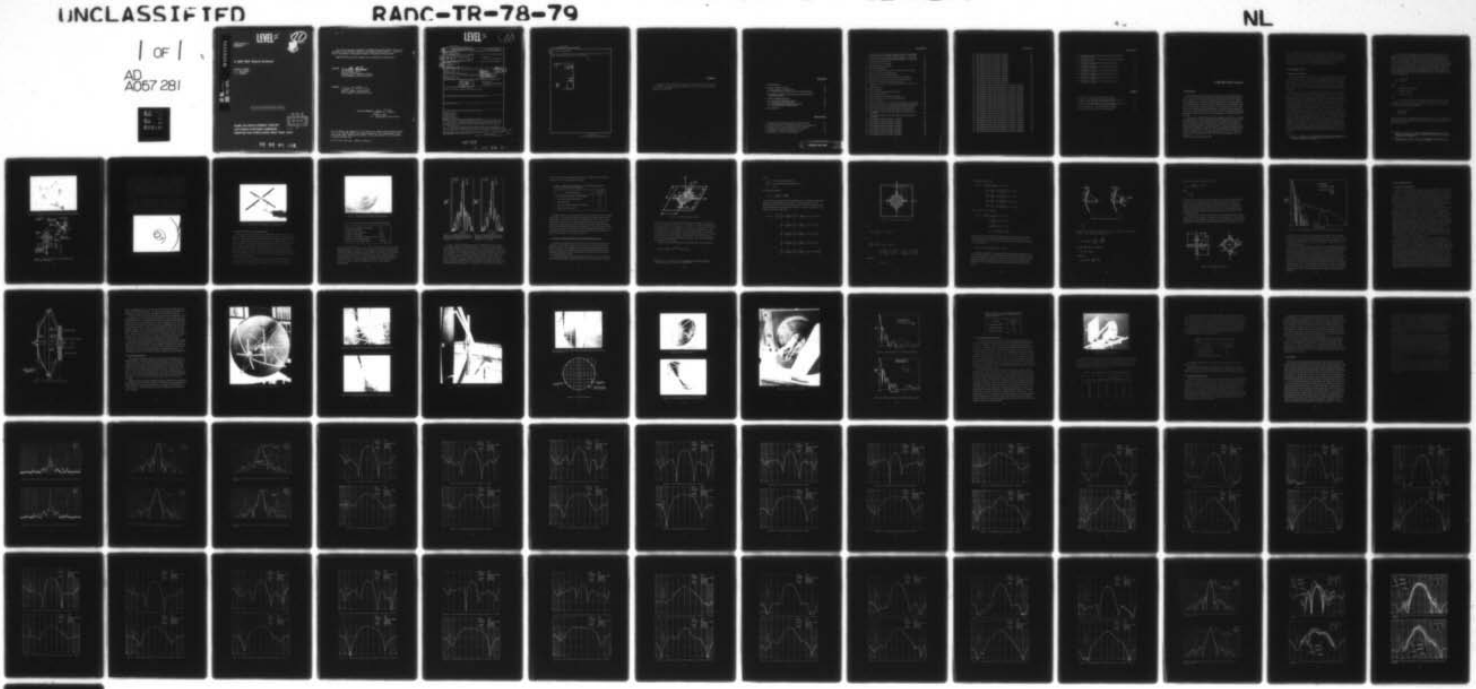

END
DATE
FILMED
9-78
DDC

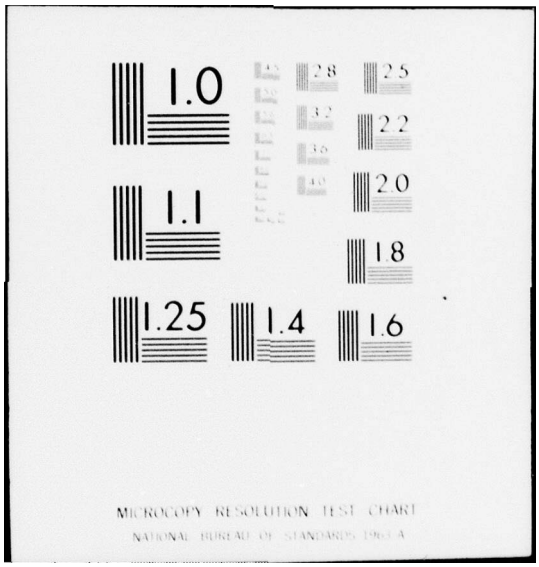
1.0
1.1
1.25
1.4
1.6
2.8
2.5
3.2
2.2
3.6
2.0
4.0
1.8
MICROCOPY RESOLUTION TEST CHART
NATIONAL BUREAU OF STANDARDS 1963-A

LEVEL II

RADC-TR-78-79
IN-HOUSE REPORT
MARCH 1978

A UHF/EHF Hybrid Antenna

JOHN A. STROM
R. J. MAILLOUX
L. F. DENNETT

ROME AIR DEVELOPMENT CENTER
AIR FORCE SYSTEMS COMMAND
GRIFFISS AIR FORCE BASE, NEW YORK 13441

This report has been reviewed by the RADC Information Office (OI) and is releasable to the National Technical Information Service (NTIS). At NTIS it will be releasable to the general public, including foreign nations.

RADC-TR-78-79 has been reviewed and is approved for publication.

APPROVED: Walter Rotman

WALTER ROTMAN, Chief
Antennas and RF Components Branch
Electromagnetic Sciences Division

APPROVED: Allan C. Schell

ALLAN C. SCHELL, Acting Chief
Electromagnetic Sciences Division

FOR THE COMMANDER: John P. Huss

JOHN P. HUSS
Acting Chief, Plans Office

If your address has changed or if you wish to be removed from the RADC mailing list, or if the addressee is no longer employed by your organization, please notify RADC (EEA), Hanscom AFB MA 01731. This will assist us in maintaining a current mailing list.

Do not return this copy. Retain or destroy.

LEVEL II

11

Unclassified

SECURITY CLASSIFICATION OF THIS PAGE (When Data Entered)

REPORT DOCUMENTATION PAGE	READ INSTRUCTIONS BEFORE COMPLETING FORM
1. REPORT NUMBER: RADC-TR-78-79	2. GOVT ACCESSION NO. / 3. RECIPIENT'S CATALOG NUMBER
4. TITLE (and Subtitle): A UHF/EHF HYBRID ANTENNA	5. TYPE OF REPORT & PERIOD COVERED: In-House
	6. PERFORMING ORG. REPORT NUMBER
7. AUTHOR(s): John A. Strom, R.J. Mailloux, L.F. Dennett	8. CONTRACT OR GRANT NUMBER(s)
9. PERFORMING ORGANIZATION NAME AND ADDRESS: Deputy for Electronic Technology (RADC/EEA), Hanscom AFB, Massachusetts 01731	10. PROGRAM ELEMENT, PROJECT, TASK AREA & WORK UNIT NUMBERS: 63431F, AFSAT201, T2
11. CONTROLLING OFFICE NAME AND ADDRESS: Deputy for Electronic Technology (RADC/EEA), Hanscom AFB, Massachusetts 01731	12. REPORT DATE: March 1978 / 13. NUMBER OF PAGES: 68
14. MONITORING AGENCY NAME & ADDRESS (if different from Controlling Office)	15. SECURITY CLASS. (of this report): Unclassified / 15a. DECLASSIFICATION/DOWNGRADING SCHEDULE

16. DISTRIBUTION STATEMENT (of this Report)

Approved for public release; distribution unlimited.

17. DISTRIBUTION STATEMENT (of the abstract entered in Block 20, if different from Report)

18. SUPPLEMENTARY NOTES

309 050

19. KEY WORDS (Continue on reverse side if necessary and identify by block number)

Hybrid antenna
Reflector antenna
UHF antenna
Aperture blockage

20. ABSTRACT (Continue on reverse side if necessary and identify by block number)

This study describes the development and experimental demonstration of the RF feasibility of combining a UHF antenna with an EHF paraboloid. The combination is to provide dual frequency band operation for air-to-satellite communication links.

A complete set of gain tables and radiation patterns are presented for a UHF crossed-dipole positioned in the aperture of two different EHF paraboloids. An analysis of the resultant blockage is described and theoretical radiation

→ next page

DD FORM 1 JAN 73 1473 EDITION OF 1 NOV 65 IS OBSOLETE

Unclassified

SECURITY CLASSIFICATION OF THIS PAGE (When Data Entered)

309 050

20. Abstract (Continued)

patterns are calculated and compared with the experimental results. Fuselage simulation experiments are also included.

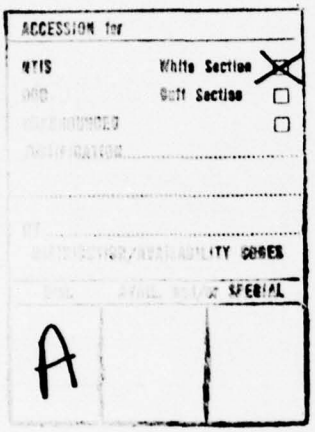

Preface

The authors wish to thank Drs. H. King and J. Wong of the Aerospace Corporation, and Mr. C. Lindberg of Lincoln Laboratory for their advice on the design and testing of the UHF dipole.

Contents

Illustrations

Illustrations

Illustrations

Tables

A UHF/EHF Hybrid Antenna

I. INTRODUCTION

The objectives of this study were the development and experimental demonstration of the RF feasibility of combining a UHF antenna with an EHF paraboloid. The combination is to provide dual frequency band operation for air-to-satellite communication links. Present airborne SATCOM systems use separate antennas for these applications. The UHF radiator is generally fixed to the fuselage, while the microwave reflector antenna is located on a steerable platform within a large radome and mechanically tracks the satellite. The problem with this approach is the low gain of the UHF antenna at the aircraft horizon. Increasing this gain would bring about a substantial improvement in performance and reliability of the UHF data link.

At the request of SAMSO (SKX) the Electromagnetic Sciences Division of RADC has undertaken this primarily experimental study of placing a rather large wide-band UHF radiator in various aperture locations of an EHF reflector antenna. Increased gain and radiation characteristics are desired at the UHF band, while minimizing the degradation to the EHF capability. The experimental program was conducted in two phases. In Phase I, a UHF crossed-dipole was designed, fabricated, and integrated with a focal point-fed paraboloid at 34.5 GHz. The UHF dipole was positioned between the focal point feed and the parabolic reflector in

(Received for publication 4 April 1978)

order to investigate the 'worst case' geometries for the combination. Section 2 describes these results. In Section 3, a simple analysis is presented to study the effects of EHF reflector blockage especially with respect to antenna gain and radiation sidelobe levels. Phase II of the experimental program explored the modification and repositioning of the UHF dipole near the focal point of a 43.5 GHz cassegrain reflector antenna. These results are detailed in Section 4.

2. PHASE I HYBRID ANTENNA

2.1 Description of the UHF Dipole

The basic requirements for the UHF radiator include an operational capability for the frequency band 293 to 400 MHz, and knowledge of radiation characteristics down to 243 MHz. Essentially, the total 225 to 400 MHz band would be examined with emphasis on the operating band. In addition to operating over a wide bandwidth, the UHF antenna is required to be circularly polarized. One dipole that satisfies these requirements is the balun-fed, open-sleeve design selected for this application.

The basic parameters influencing the balun-fed, open-sleeve crossed dipole have been investigated in great detail by Wong and King.[1] This work forms the basis of our design. *Their studies have shown that with the addition of parasitic* elements (sleeves) to the conventional cylindrical dipole, the VSWR bandwidth can be broadened significantly with negligible changes in the radiation padterns. The open sleeve dipole can operate over a 1.8:1 frequency bandwidth as compared to 1.25:1 for the cylindrical dipole. The sleeve necessary to compensate for the required bandwidth of a crossed-dipole must be of the circular disk or Greek-Cross shape in order to provide circular symmetry. The cross-sectional area of the crossed dipole including its sleeve, has a direct relationship on any gain decrease to the EHF reflector antenna's radiation characteristics when the dipole is positioned near the radiating aperture of the reflector. The EHF gain is reduced and the resultant radiation pattern sidelobe are increased when the blockage is introduced. The relatively large size of the UHF dipole (20 in.) with respect to the diameter of the parabolic reflector (39.4 in.) dictates that a substantial gain reduction can be anticipated. An additional negative effect also occurs when the position of the dipole is between the focal point feed and the reflector, as is the 'worst case' blockage of this Phase I study. The position effect is discussed in Section 3.

---

1. Wong, J. L., and King, H. E. (1973) Design Variations and Performance Characteristics of the Open-Sleeve Dipole, Report SAMSO-TR-73-133, The Aerospace Corporation, El Segundo, Ca.

In order to reduce the blockage effects, the UHF dipole and its sleeve were designed using wire-grid construction.[2] A photograph of this design is shown in Figure 1. The construction details of the crossed, open-sleeve dipole and its balun are given in Figure 2. The wire-grid assembly of the Greek-cross shaped compensation sleeve consists of 0.0625 in. brass rods spaced 1.0 in. and soldered to a 0.125 in. $\times$ 0.125 brass frame. This construction simulates a solid metallic surface. The dipole elements are also designed using wire grid or "cage" techniques which has been described in Schelkunoff and Friis.[3] When the wires are thin and equispaced, the "cage" structured dipole will replace a cylindrical dipole according to expression

$$r_{eff} = r \left(\frac{n\, r_o}{r} \right)^{1/n}$$

where

r = radius of the wire "cage"

n = number of wires

r_o = radius of the wires

and

r_{eff} = the effective radius of the solid dipole replaced by the "cage" dipole.

Conversely, if the cylindrical dipole radius has been determined, the radius of the "cage" dipole replacement would be

$$r = \left[\frac{r_{eff}}{(n\, r_o)^{1/n}} \right]^{n/n-1} .$$

The effective radius of the dipole shown in Figure 2 is 0.567 in. The dipole length was determined experimentally by optimizing VSWR response over the UHF frequency band of interest.

---

2. King, H.E., and Wong, J.L. (1972) 225-400 MHz Antenna System for Spin Stabilized Synchronous Satellites, Report SAMSO-TR-72-77, The Aerospace Corporation, El Segundo, CA.

3. Schelkunoff, S.A., and Friis, H.T. (1952) Antennas: Theory and Practice, John Wiley and Sons, Inc., New York, pp 110-111.

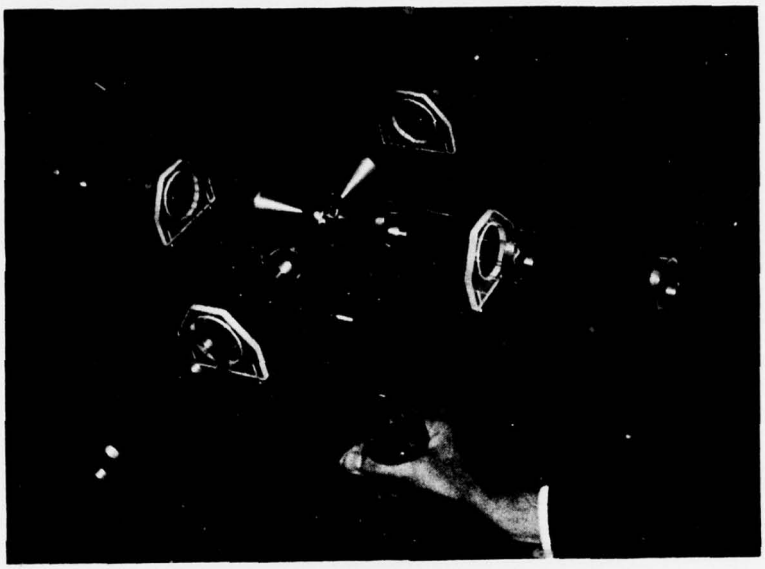

Figure 1. Photograph of UHF Dipole Using Wire Grid Construction

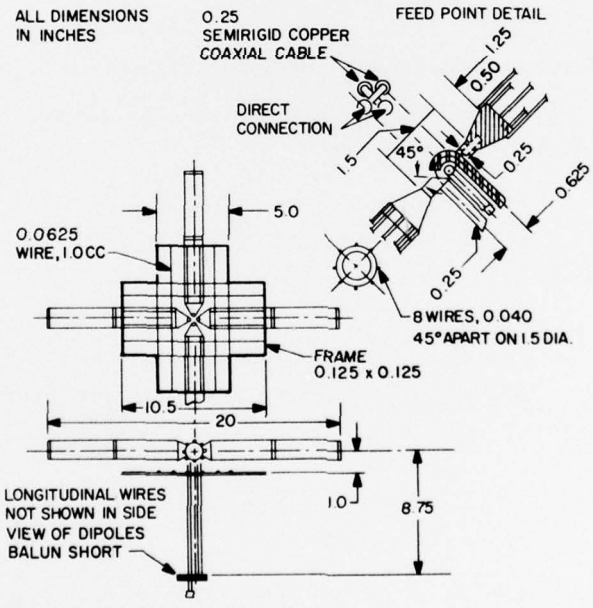

Figure 2. Construction Details of UHF Dipole Using Wire Grid Construction

The dipole feed line is fabricated of copper-clad 0.25 in. diameter semi-rigid coaxial cable. The balanced line of the balun is also a length of this cable but does not use the center conductor. The balun short of the feed-balun line combination is normally spaced one quarter wavelength from the input terminals of the dipole elements. Here again, this dimension has been adjusted experimentally to optimize VSWR over the frequency band. An approximate 4:1 impedance transformation is realized with this balun design. Plexiglas spacers (see Figure 1) fitted over the dipoles provide support for the sleeve. A typical Smith Chart plot of impedance for this dipole is traced in Figure 3 over the frequency band 225 to 400 MHz.

For purposes of comparison, a second set of dipole elements was also fabricated using 1 in. diameter tubular aluminum. Figure 4 shows a photograph of the UHF dipole using solid elements and the same wire-grid sleeve as before. The sleeve spacing has been reduced to 0.75 in. for a more optimal VSWR bandwidth. These measurements, of course, as well as those for the cage dipoles have been performed with the balun short coincident with the surface of the reflector.

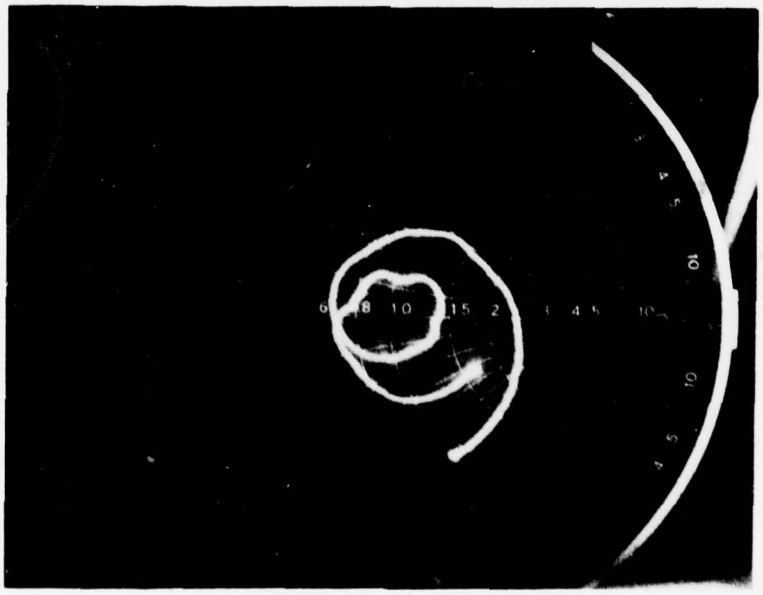

Figure 3. Impedance Plot of UHF Cage Dipole for 225 to 400 MHz

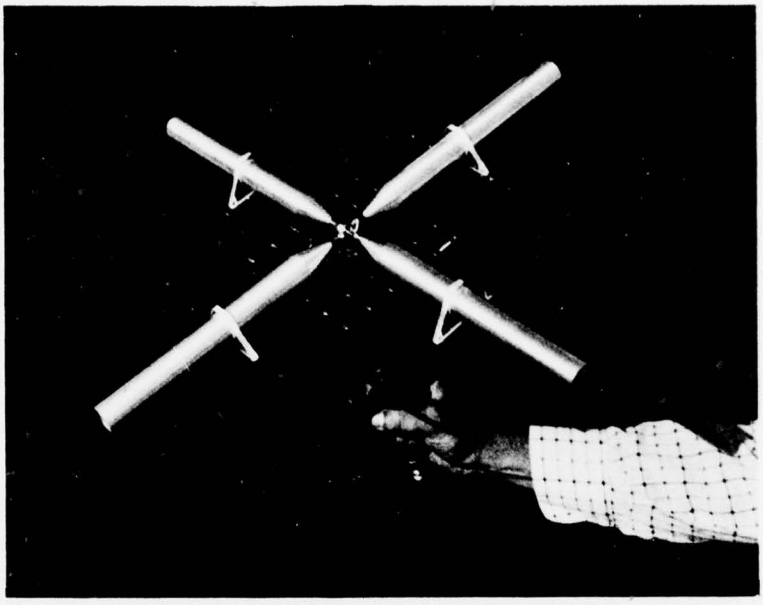

Figure 4. Photograph of UHF Dipole Using Solid Elements

2.2 Radiation Characteristics for the Combination Antenna

The Phase I hybrid antenna combines the UHF dipole with a 1 meter diameter EHF (34.5 GHz) parabolic reflector antenna as shown in Figure 5. The location of the dipole, approximately midway between the EHF focal point feed and the reflector surface, is obviously positioned poorly with regard to operation at EHF. However, this location does provide a good point to test the leakage effects or invisibility of the grid sleeve and cage dipole to the EHF radiation. The wire-grid spacings as seen by the EHF radiated wave vary from approximately 0.5 in. for the dipole elements to 1 in. for its sleeve. These dimensions are somewhat larger than the wavelength at EHF ($\lambda \approx 0.342$ in.) and, thus, some EHF radiation would be expected to pass through the structure. Table 1 lists the more important dimensions of the Phase I combination antenna.

In order to test the UHF dipole's interference, far-field radiation patterns and relative gain measurements at 34.5 GHz for the EHF reflector antenna were performed with and without the dipole installed. The resultant E- and H-plane

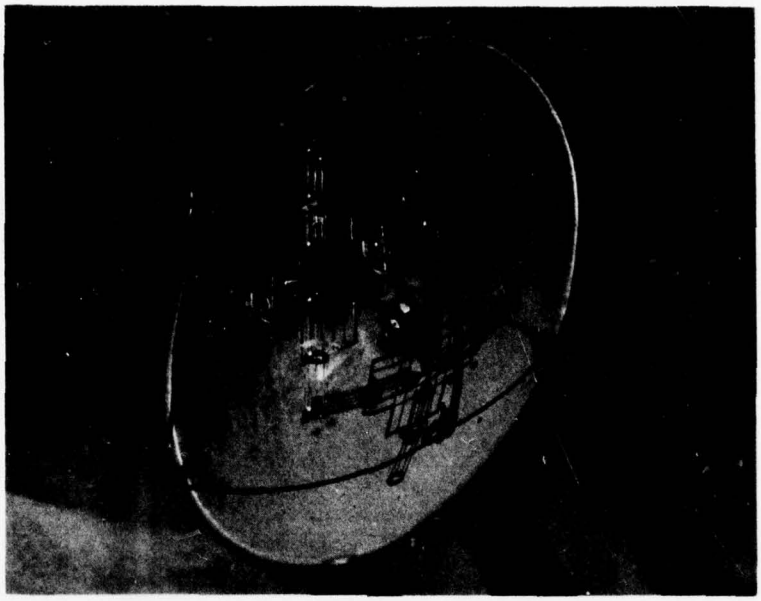

Figure 5. Photograph of the Phase I Hybrid Antenna

Table 1. Dimensions of Phase I UHF/EHF Hybrid Antenna

EHF Parabolic Reflector Diameter:	1 m
Focal Distance (f/D):	0.4
Spacing of EHF Feed Horn:	0.37 m
Length of UHF Dipole:	20 in.
Spacing of UHF Dipole to Reflector Surface:	8.75 in.
Diameter of UHF Caged Dipoles:	1.5 in.
Dimensions of UHF Dipole Sleeve:	See Figure 2

patterns are traced in Figures 6 and 7. These plots indicate the normal operation without UHF dipole as solid lines, while the dashed curves are superimposed and reflect the quantitative changes due to the influence of the dipole. The dipole addition reduces the unobstructed boresight gain of 47.6 dBi by 2.0 dB, while the angular width of the main beam is narrowed slightly and significantly higher sidelobe levels result. All pattern and gain measurements were performed over a 1/2 mile free space range at the RADC Antenna Test Facility, Ipswich, Massachusetts.

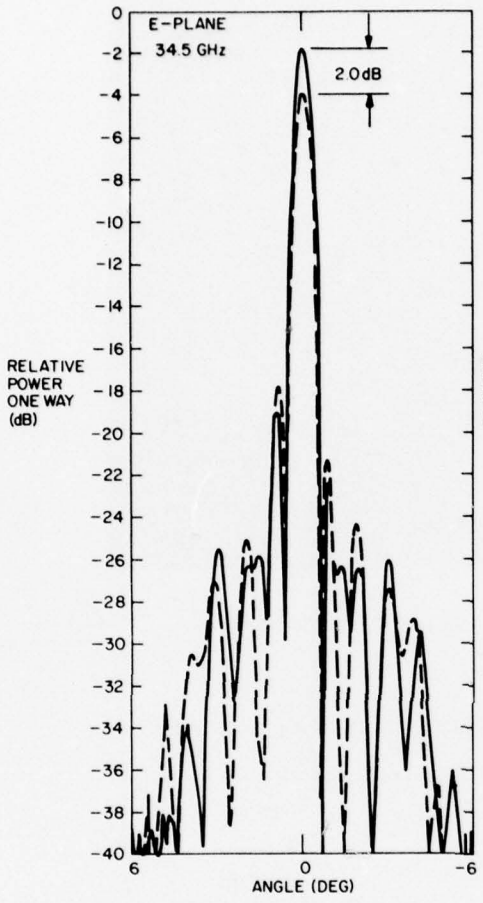

Figure 6. Radiation Patterns of the EHF Parabolic Reflector Antenna With and Without the UHF Dipole Attached (E-Plane, f = 34.5 GHz)

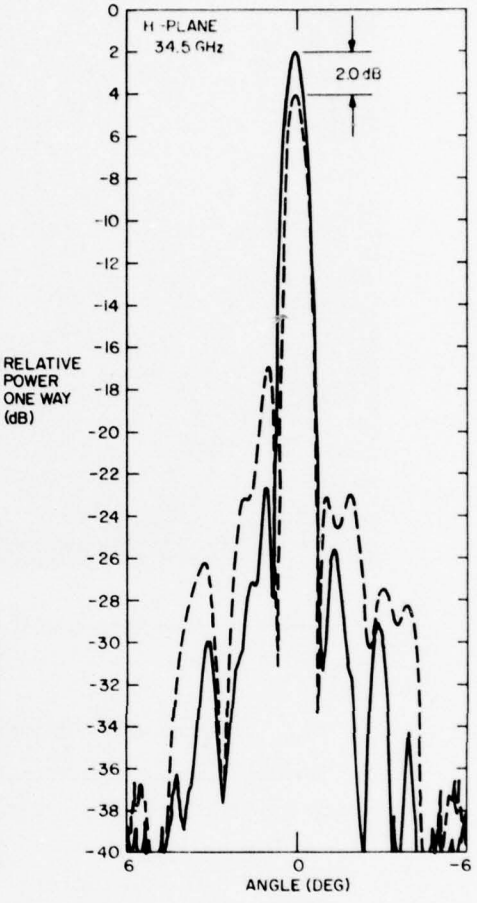

Figure 7. Radiation Patterns of the EHF Parabolic Reflector Antenna With and Without the UHF Dipole Attached (H-Plane, f = 34.5 GHz)

In order to identify the dipole components contributing the major portion of the blockage at EHF in the combination antenna, a series of structural changes were made to the dipole. First, the grid sleeve was removed with all other parameters unchanged. No noticeable differences to either the EHF patterns or the gain were observed. As a second step, the cylindrical dipole elements shown in Figure 4 were substituted for the "caged" elements of Figure 1, again without the sleeve. Likewise, no change in the EHF patterns and gain level was noticed. Finally, the dipole elements were removed completely, leaving only the balun and feed cables fixed in the parabola. This resulted in a 1.3 dB increase in the gain

level over that with the complete dipole structure. Table 2 summarizes these changes and the corresponding gain variations.

Table 2. Influence of the UHF Dipole on the EHF Boresight Gain of the Phase I UHF/EHF Hybrid Antenna

Antenna Condition	Gain (dBi)
EHF Parabolic Antenna (No UHF Dipole)	47.6
Cage Dipole Added (See Figure 5)	45.6
Sleeve Removed	45.6
Cylindrical Dipoles Substituted (No Sleeve)	45.6
Dipole Elements Removed	46.9

Radiation patterns for the UHF range were also measured, but are not included in this report. Generally, these patterns had directive radiation characteristics yielding gains of 4 to 7 dBi over the 225 to 400 MHz band. The geometric configuration of the strut support for the focal-point feed horn, however, presents unsymmetric interference to the UHF radiation which would be especially significant for the intended circularly polarized application. These unsymmetries could be observed in E- and H-plane patterns for the individual orthogonal dipoles. The capability for making circular polarized patterns and axial ratio measurements for these frequencies was not available at this time.

3. ANALYSIS OF APERTURE BLOCKAGE FOR THE UHF/EHF HYBRID ANTENNA

The UHF crossed dipole with its Greek-Cross sleeve presents a fairly large obstruction to the directed radiation from the EHF horn of the Hybrid Antenna. The effective area of this blockage and its respective location geometries have a direct relationship to the degradation or gain losses at the EHF band. By using techniques such grid and "caged" construction, the blockage may be reduced for more acceptable EHF operation.

In analyzing the effect of blockage depicted in Figure 8, it is assumed that the EHF feed system energy associated with the shaded area is absorbed or scattered

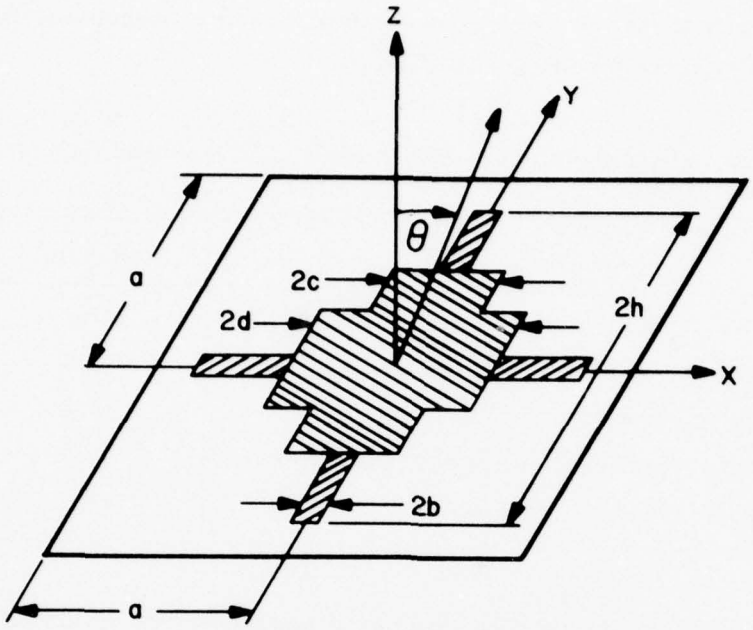

Figure 8. Aperture Blockage Geometry

in such a way that its contribution to the axial gain is negligible.[4] The shaded area refers specifically to the 'worst' case blockage of a UHF crossed-dipole using solid metallic elements and sleeve. Similarly, it is assumed that the effect on the unshaded area is also negligible. The rectangular coordinate system and square aperture are used to simplify the blockage calculations. Since, however, the separable aperture illumination is nearly circular, the dimension "a" may be associated with one half the diameter of the parabola. The far field radiation pattern in the principal plane (defined to include the y and z axes) is evaluated in the remainder of this section.

The un-normalized field pattern for these geometries may be expressed as

$$E(x, y, \theta) = \int f(x, y)\, e^{jk_o y \sin\theta}\, B(x, y)\, dx\, dy$$

---

[4] Rusch, W. V. T., and Potter, P. D. (1970) Analysis of Reflector Antennas, Academic Press, Inc., New York, pp 82-106.

where

$f(x, y)$ = the area illumination function,

$B(x, y)$ = the unblocked radiating aperture, and

$k_o = 2\pi/\lambda$.

The illumination function

$$f(x, y) = \cos\left(\frac{\pi x}{2a}\right) \cos\left(\frac{\pi y}{2a}\right)$$

is chosen because its nearly circular distribution and its resultant sidelobe levels approximate the operating characteristics of a typical EHF parabola. The unblocked area $B(x, y)$ is symmetric with respect to the x and y coordinates, and may be integrated by summing the area integrals as indicated in Figure 9. The integral may now be expressed as:

$$E(x', y', \theta) = 4 \left\{ 0 + \int_o^b \cos\left(\frac{\pi x'}{2a}\right) dx' \int_h^a \cos\left(\frac{\pi y'}{2a}\right) \cos(k_o y' \sin\theta)\, dy' \right.$$

$$+ \int_b^c \cos\left(\frac{\pi x'}{2a}\right) dx' \int_d^a \cos\left(\frac{\pi y'}{2a}\right) \cos(k_o y' \sin\theta)\, dy'$$

$$+ \int_c^d \cos\left(\frac{\pi x'}{2a}\right) dx' \int_c^a \cos\left(\frac{\pi y'}{2a}\right) \cos(k_o y' \sin\theta)\, dy'$$

$$+ \int_d^h \cos\left(\frac{\pi x'}{2a}\right) dx' \int_b^a \cos\left(\frac{\pi y'}{2a}\right) \cos(k_o y' \sin\theta)\, dy'$$

$$\left. + \int_h^a \cos\left(\frac{\pi x'}{2a}\right) dx' \int_o^a \cos\left(\frac{\pi y'}{2a}\right) \cos(k_o y' \sin\theta)\, dy' \right\} .$$

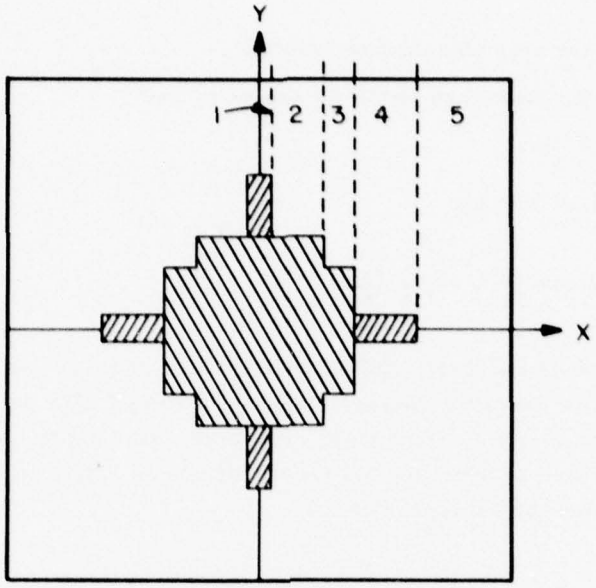

Figure 9. Symmetric Areas of Blockage

But

$$\int \cos\left(\frac{\pi x'}{2a}\right) dx' = \frac{2a}{\pi} \sin\frac{\pi x'}{2a}$$

and

$$\int \cos\left(\frac{\pi y'}{2a}\right) \cos\left(k_o y' \sin\theta\right) dy' =$$

$$= \left[\frac{\sin\left(\frac{\pi}{2a} - k_o \sin\theta\right) y'}{2\left(\frac{\pi}{2a} - k_o \sin\theta\right)} + \frac{\sin\left(\frac{\pi}{2a} + k_o \sin\theta\right) y'}{2\left(\frac{\pi}{2a} + k_o \sin\theta\right)}\right]$$

By definition

$$= \frac{1}{2}\, \eta(\theta, y')$$

The integral now becomes:

$$E(x', y', \theta) = \frac{4a}{\pi} \left\{ \sin\left(\frac{\pi b}{2a}\right)[\eta(\theta, a) - \eta(\theta, h)] \right.$$

$$+ \left[\sin\left(\frac{\pi c}{2a}\right) - \sin\left(\frac{\pi b}{2a}\right)\right][\eta(\theta, a) - \eta(\theta, d)]$$

$$+ \left[\sin\left(\frac{\pi d}{2a}\right) - \sin\left(\frac{\pi c}{2a}\right)\right][\eta(\theta, a) - \eta(\theta, c)]$$

$$+ \left[\sin\left(\frac{\pi h}{2a}\right) - \sin\left(\frac{\pi d}{2a}\right)\right][\eta(\theta, a) - \eta(\theta, b)]$$

$$\left. + \left[\sin\left(\frac{\pi a}{2a}\right) - \sin\left(\frac{\pi h}{2a}\right)\right][\eta(\theta, a) - \eta(\theta, o)] \right\} .$$

This equation may be reduced to:

$$E(x', y', \theta) = \frac{4a}{\pi} \left\{ \sin\left(\frac{\pi b}{2a}\right)[\eta(\theta, d) - \eta(\theta, h)] \right.$$

$$+ \sin\left(\frac{\pi c}{2a}\right)[\eta(\theta, c) - \eta(\theta, d)]$$

$$+ \sin\left(\frac{\pi d}{2a}\right)[\eta(\theta, b) - \eta(\theta, c)]$$

$$\left. + \eta(\theta, a) - \sin\left(\frac{\pi h}{2a}\right)[\eta(\theta, b)] \right\} .$$

We now have a general equation for the field pattern with open-sleeve crossed dipole blockage. This equation will handle the special cases when the sleeve is removed or altered in size or shape. The normalized power pattern as a function of θ is expressed as:

$$P(x', y', \theta) = 20 \log \left\{ \left(\frac{\pi}{4a}\right)^2 [E(x', y', \theta)] \right\} .$$

A problem encountered in locating the UHF dipole between the EHF feed horn and the reflector surface, is that the dipole casts a shadow on the reflector surface when it is illuminated by the horn. Figure 10 describes the geometries for a parabola (Figure 10a) and a parabola with a shadow cast on its surface (Figure 10b). In Figure 10a, the general equation describing the reflector in terms of its focal point is

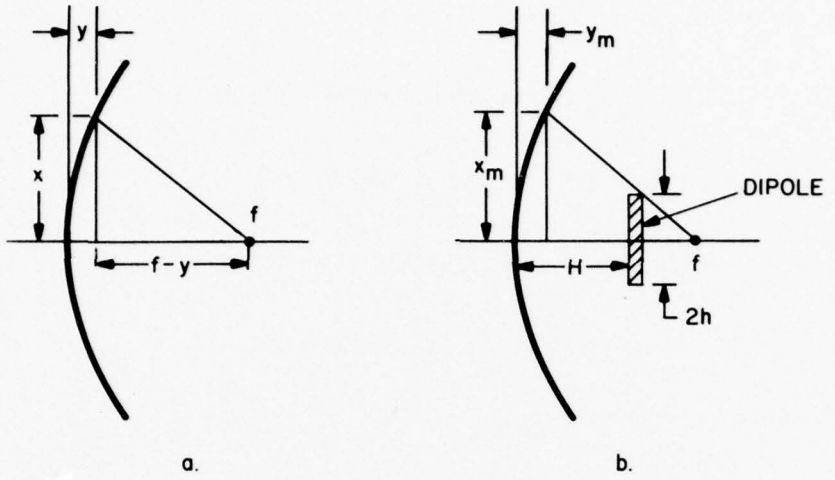

Figure 10. Parabolic Reflector Geometry

$$y = \frac{x^2}{4f} \quad .$$

In Figure 10b, a dipole is mounted a distance H from the surface. The dipole of height, h, casts a shadow of height x_M. Let

$$R = \left(\frac{f - H}{h}\right) = \frac{f - y_M}{x_M} = \frac{f - \frac{x_M^2}{4f}}{x_M} \quad .$$

This equation may be re-written as

$$4f^2 - x_M^2 = 4f x_M R$$

and finally

$$x_M = 2f \left[- R \pm \sqrt{R^2 + 1} \right]$$

but x_M must have a positive value. Therefore

$$x_M = 2f \left[\sqrt{R^2 + 1} - R \right] ,$$

where

$$R = \frac{(f - H)}{h} .$$

This expression is referred to as the magnification factor describing the height of a shadow cast by a dipole located H from the parabolic surface. If the same analysis is used to calculate the shadow cast by the dipole width, a complete straight line description of the "blocked" area of the surface can be determined. Because of the relative flatness of the reflector surface of the Phase I antenna, the blocked area has been analyzed without including the added complexity of the parabolic curvature.

The Phase I EHF radiation performance has been calculated using the magnification factor for two conditions of blockage described in Figure 11. These include the solid crossed-dipole (Figure 11a) and the same dipole with a solid sleeve added (Figure 11b). The resultant computed radiation patterns are plotted in Figure 12.

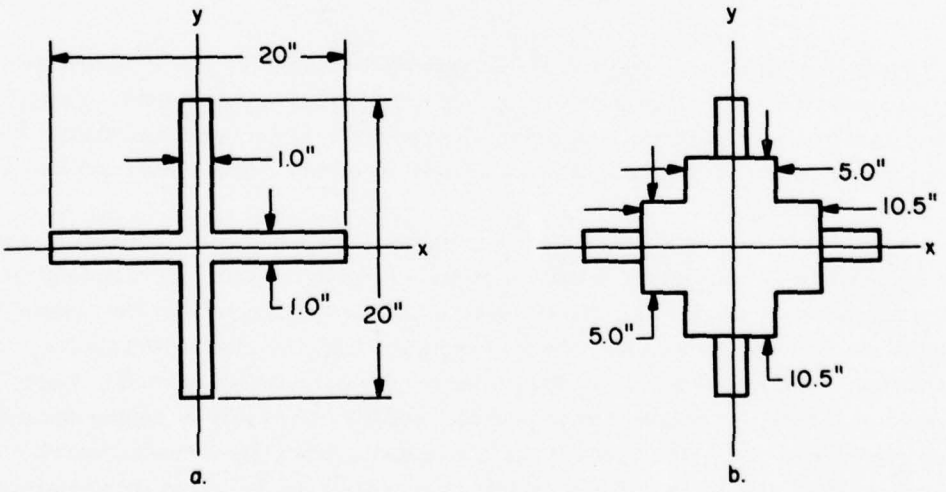

Figure 11. Examples of Blockage

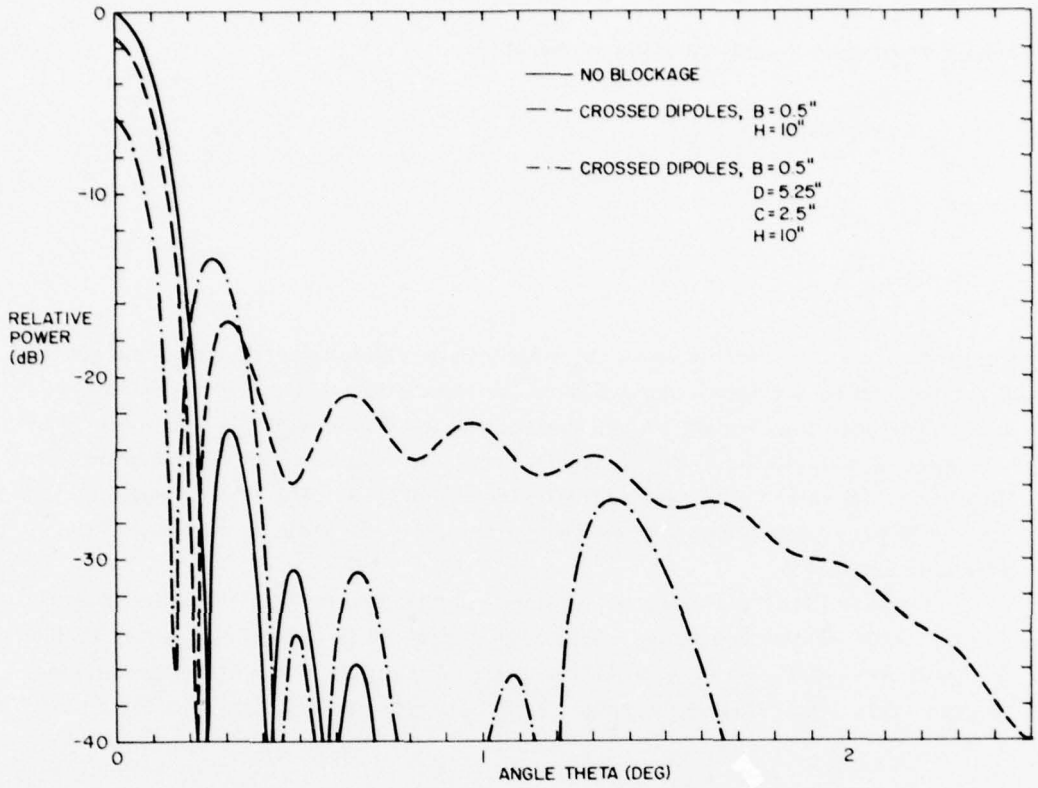

Figure 12. Calculated Radiation Patterns for the Phase I Hybrid Antenna

Introduction of crossed-dipoles to the antenna system reduces the boresight gain by approximately 1.6 dB over the unblocked case. In addition, sidelobe energy levels are raised substantially at small angular displacements off boresight. With the addition of the solid sleeve, the directional radiation characteristics become obviously unacceptable.

When these computed results are compared to the experimental measurements of Section 2.2, a similiarity in the variations to the gain levels and radiation pattern shape can be observed. These observations would suggest that the "caged" dipole element design does not increase radiation transmission or reduce the cross-sectional blockage, when substituted for the solid dipole element. More research in wider wire spacings is probably needed before this technique could be recommended. More effective results are obtained when the sleeve is tested. Removal from the dipole in the boresight gain experiment indicates no noticeable change in the gain level. The computed plot of Figure 12 using a solid dipole and solid sleeve, however, dictates a gross effect to the gain. It can be assumed that the grid sleeve design is almost invisible and does reduce the blockage problem effectively.

4. PHASE II HYBRID ANTENNA

4.1 Description of UHF/EHF Antenna

The Phase II UHF/EHF Hybrid Antenna consists of an EHF cassegrain reflector antenna in combination with a variation of the UHF dipole of Section 2. Figure 13 shows a cross-sectional view of this antenna chosen in order to reduce the magnitude of the dipole blockage effects experienced in the Phase I measurements. The double reflector technique allows the UHF dipole to be repositioned behind the sub-reflector and thus out of the converging field at the EHF reflector focus, eliminating the magnified shadow effect. The blockage created by the UHF dipole's presence is equal to the dipole dimensions for the cassegrain geometry.

The EHF antenna consists of a 36 in. diameter main reflector with a 4.125 in. diameter sub-reflector illuminated by a conical feed horn protruding axially through the main reflector surface. The main reflector is a paraboloid and the auxiliary reflector is a hyperboloid. The geometry of this horn-reflector combination needed in order to collimate the radiation, requires that the feed horn be positioned at the near focus of the hyperboloid and that the focus of the paraboloid and far focus of the hyperboloid be coincidental. Cassegrain antennas are usually recommended at frequencies where feed waveguide attenuation is appreciable and where the aperture is large enough to produce a beamwidth of 1 degree or less. Sidelobes are nominally -18 dB with aperture efficiencies of 50 percent. This antenna which is readily available commercially (TRG Model B821-36-C), has an operating frequency of 43.5 GHz ± 3 percent, a boresight gain of approximately 49 dB referred to an isotropic radiator, a half-power beamwidth of about 0.5 degree and the capability of circular polarization.

The UHF portion of the Phase II Hybrid Antenna has been redesigned to be compatible with the EHF cassegrain antenna. As may be seen in Figure 13, the dipole has been repositioned outside the sub-reflector approximately at the focal point of the paraboloid. The fundamental dipole dimensions including length, diameter, and sleeve size have been retained from the Phase I conditions. The supporting rod for the cassegrain sub-reflector, normally machined as a single metallic unit was redesigned and fabricated of plexiglas dielectric so that the balun and feed cable section of the UHF dipole could be machined into its core. The cross-sectional diameter of the UHF feed network was reduced by replacing the 0.25 in. diameter coaxial cables of the Phase I dipole (see Figure 2) with 0.141 in. diameter semirigid cables and recalculating the correspondingly smaller cable separation. This new support was fitted to the strut system holder for limited axial adjustment. Because of the close proximity of the sleeve to strut system and the resultant instability of the structure, a new sleeve was fabricated with 0.125 in.

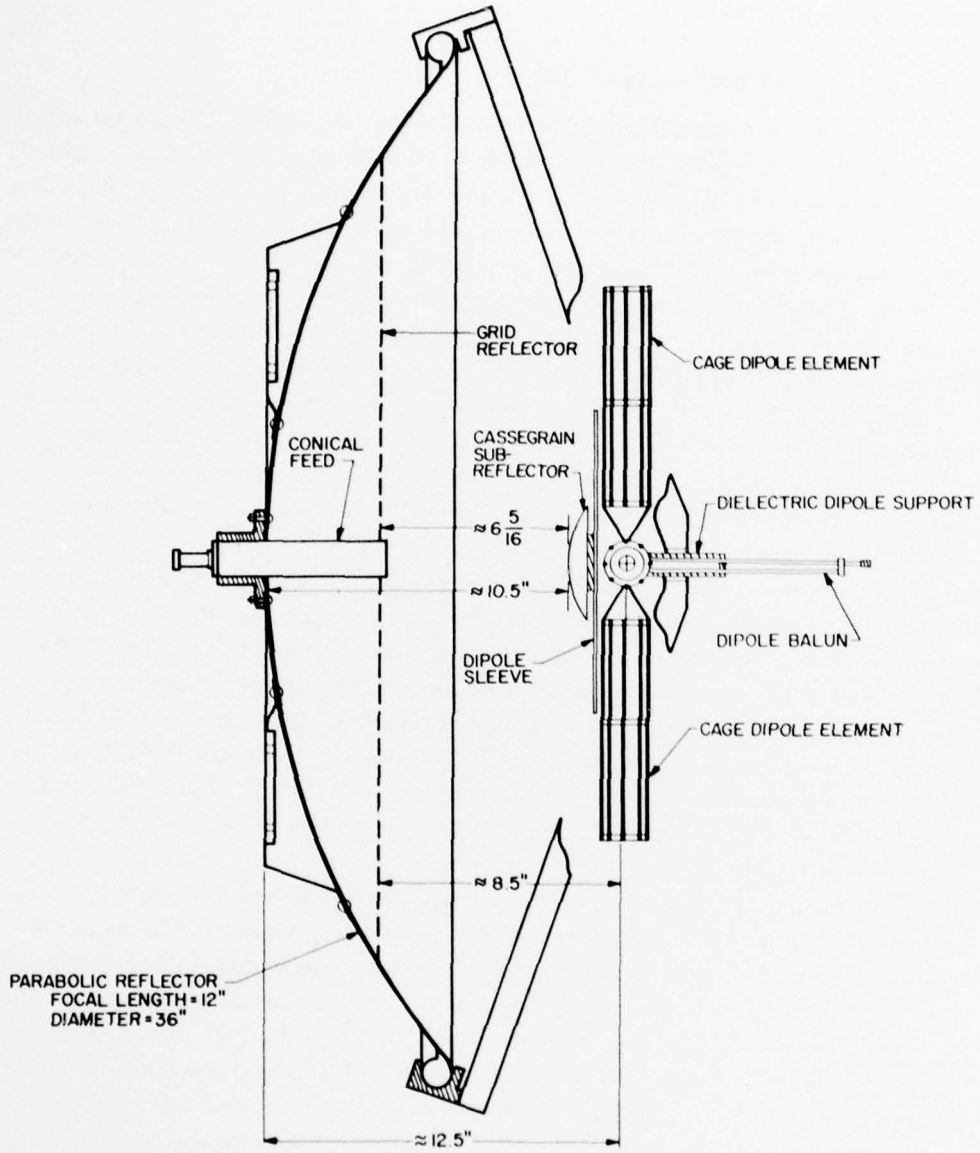

Figure 13. Phase II UHF/EHF Hybrid Antenna

square rod replacing the wires and was repositioned between the UHF dipole elements and the EHF sub-reflector. The sleeve was then fastened to both, to provide greater strength to the entire sub-reflector-UHF dipole combination.

One of the problems anticipated at UHF operation was the effectiveness of the main reflector and its directional gain characteristics when combined with relatively large dipole. An alternate reflector scheme was devised and implemented in the form of a widely spaced flat grid of wires, installed across the face of the paraboloid and located approximately one quarter wavelength from the UHF dipole at the midband frequency. The wire-grid spacing equals approximately 0.1λ at 400 MHz. Figures 14 to 18 show several photographs of close views of the UHF dipole including both solid or caged elements and the various reflector combinations. The dimensions of the UHF wire grid are described in Figure 19, while its relative location in the paraboloid is indicated by the dashed line of Figure 13. Figures 20 and 21 show both reflector variations of the Phase II antenna.

By using a conical feed horn (TRG Model B876) as the primary EHF radiator, the symmetrical geometries needed for circularly polarized operation are available. The proper series addition of such waveguide components as an orthomode transducer, circular polarizer or mode transition with the feed horn allows the measurement of right-or-left-hand circular or dual-linear polarization. The waveguide components used for Phase II Hybrid Antenna are shown in Figure 22.

4.2 Calculated Radiation Patterns

The analytical techniques developed in Section 2 are also applicable to the Phase II Antenna. Because of relocation, the UHF dipole in the new structure is illuminated by plane wave radiation and the magnification factor of the Phase I antenna is no longer needed. The blockage parameters to be used in the power pattern equation are simply the cross-sectional dimensions of the dipole. Figure 23 is a plot of the EHF radiation patterns for similar conditions as those plotted for the Phase I antenna in Figure 12. In this case the EHF reference pattern, however, includes the paraboloid with the sub-reflector as indicated by the solid curve. Table 3 lists the boresight gain changes due to the two cases of blockage.

Radiation characteristics for the EHF frequency band have been calculated and are plotted in Figure 24. These curves for 43.5 GHz, 42 GHz, and 45 GHz have been referenced to the cassegrain antenna at f_o using the solid UHF dipole and sleeve blockage. Gain level variations reflect the changes in area illumination due to frequency.

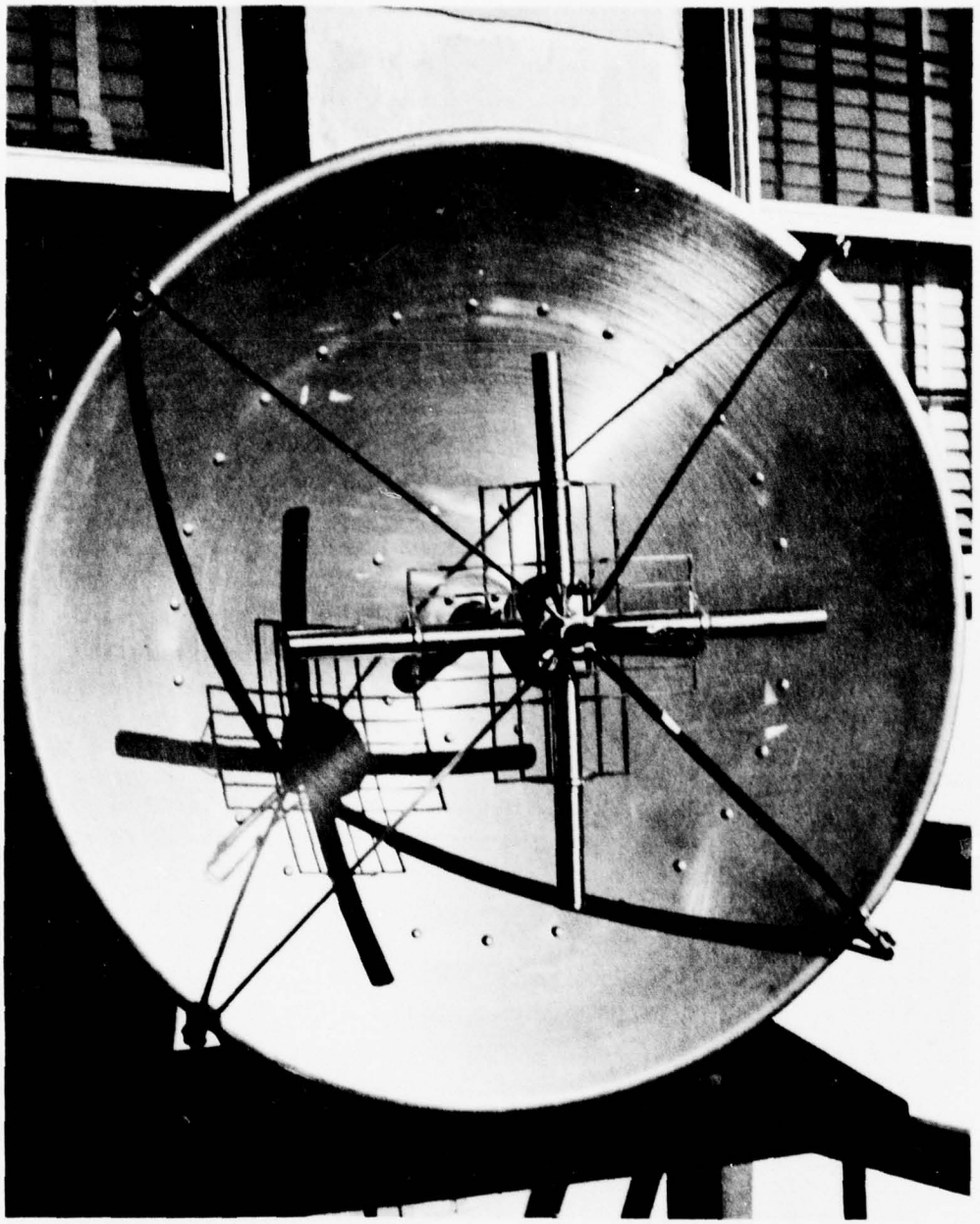

Figure 14. Front View of Phase II Hybrid Antenna

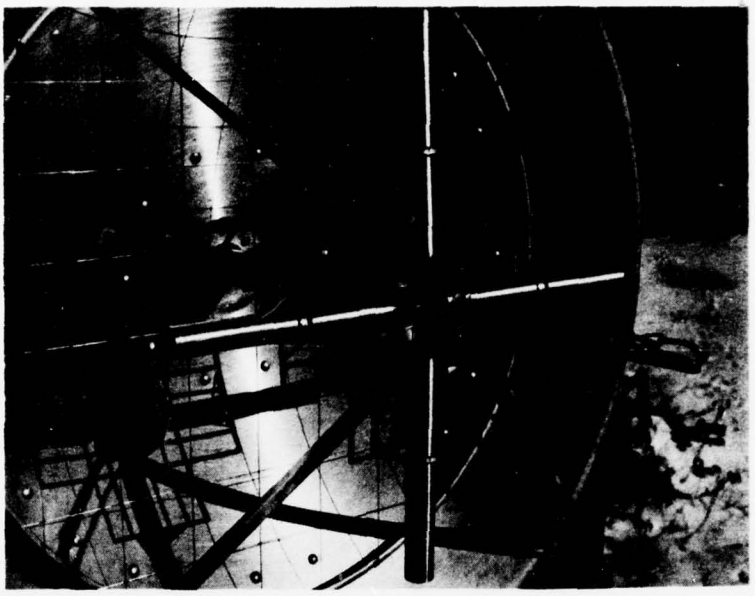

Figure 15. UHF Dipole With Solid Elements and UHF Grid Reflector

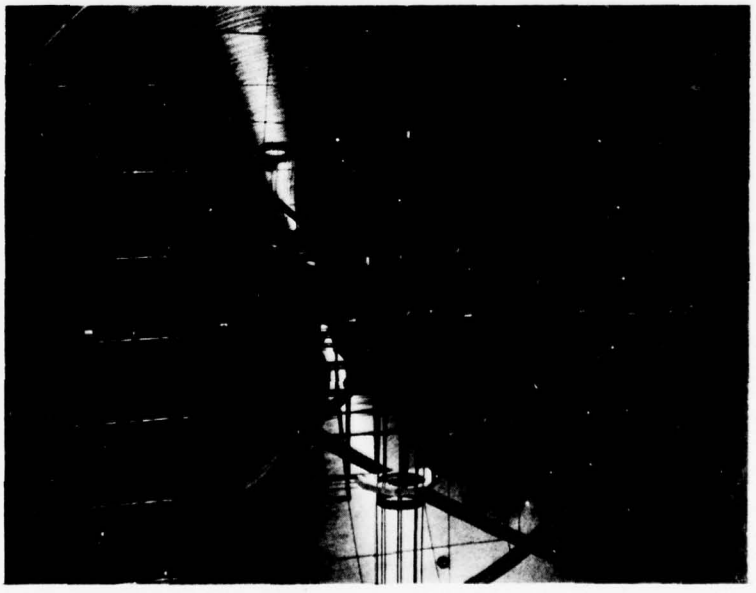

Figure 16. UHF Dipole With Caged Elements and UHF Grid Reflector

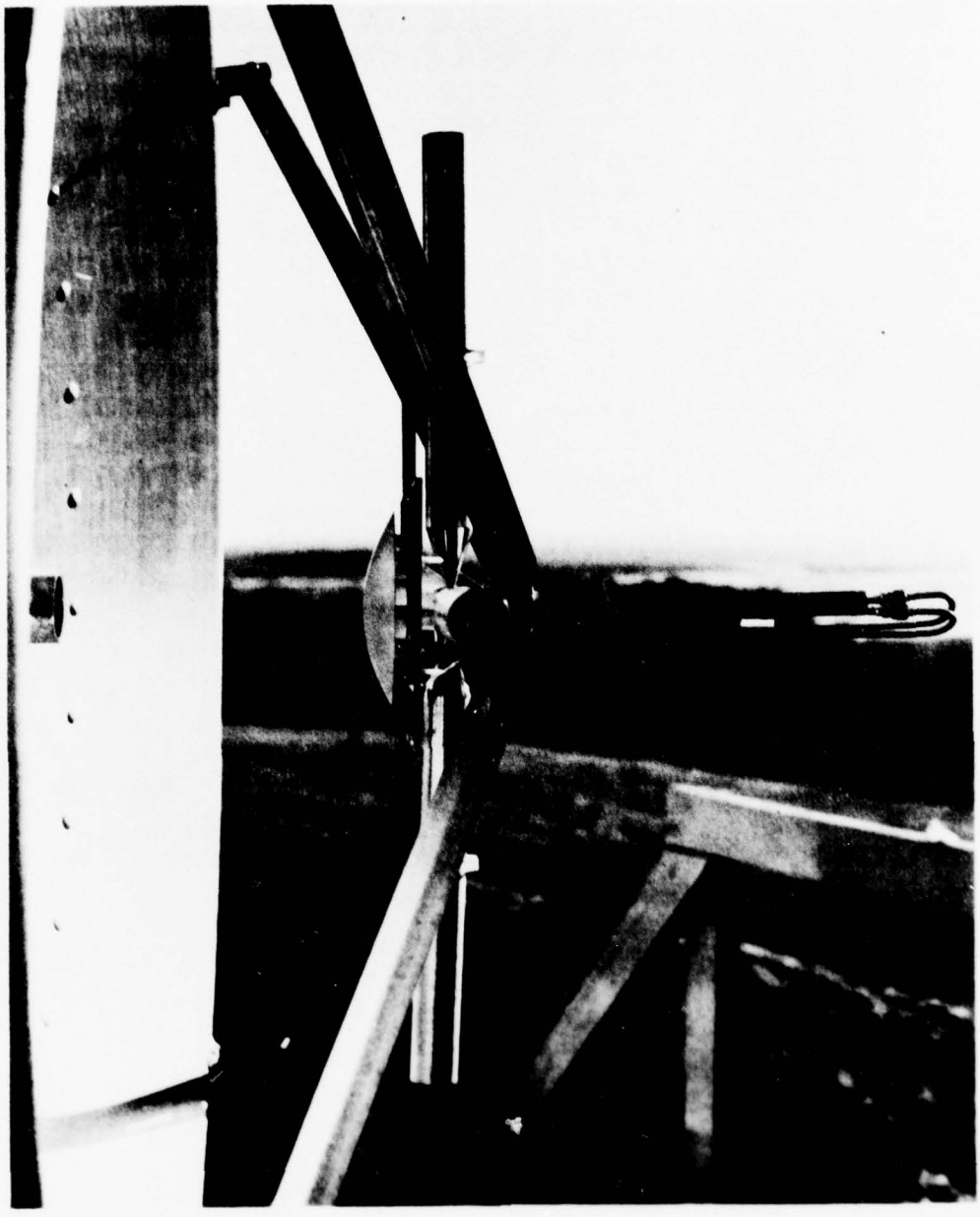

Figure 17. Side View of UHF Dipole and EHF Sub-Reflector

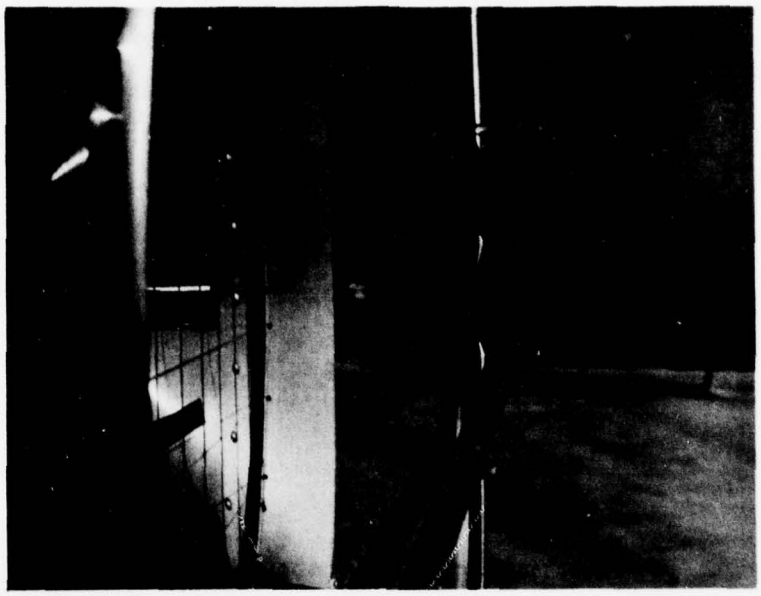

Figure 18. Side View of UHF Dipole and EHF Sub-Reflector with UHF Grid Reflector

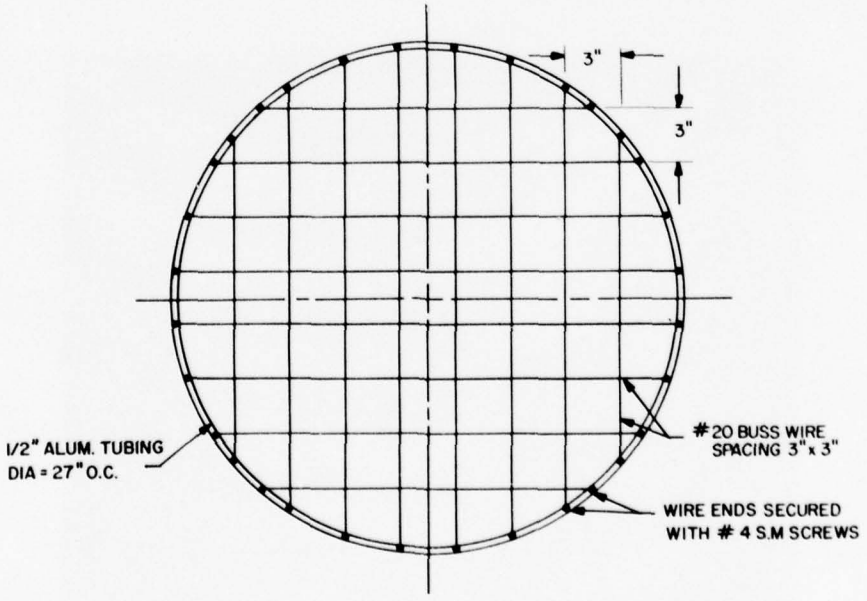

Figure 19. UHF Grid Reflector

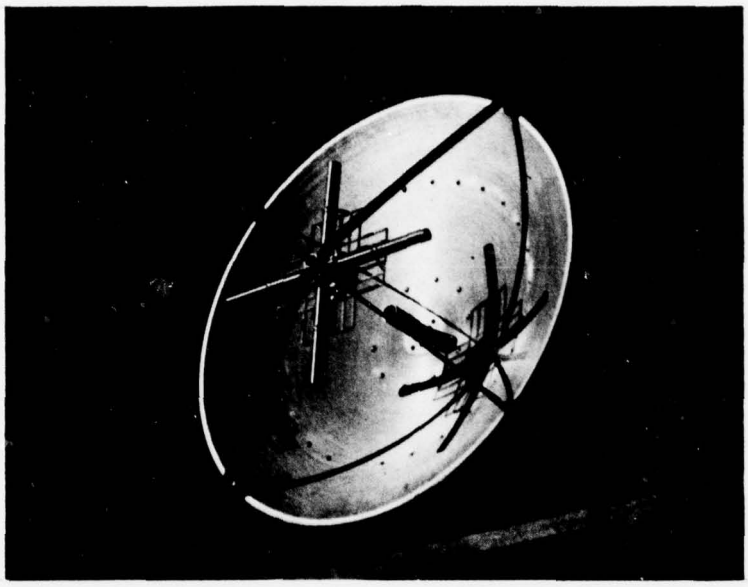

Figure 20. Phase II Antenna

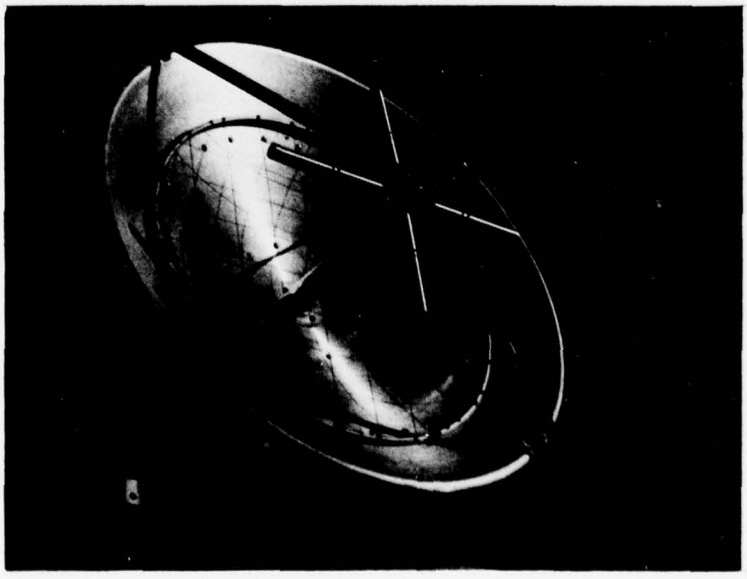

Figure 21. Phase II Antenna With UHF Grid Reflector

Figure 22. EHF Waveguide Network

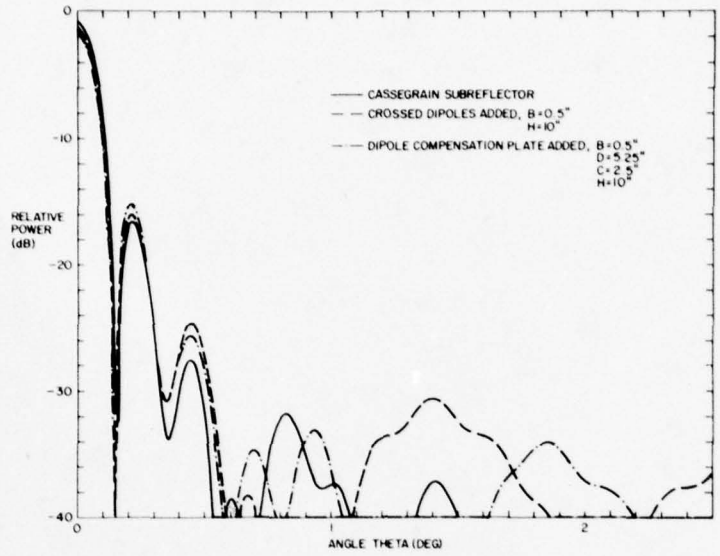

Figure 23. Radiation Patterns of the Phase II Antenna

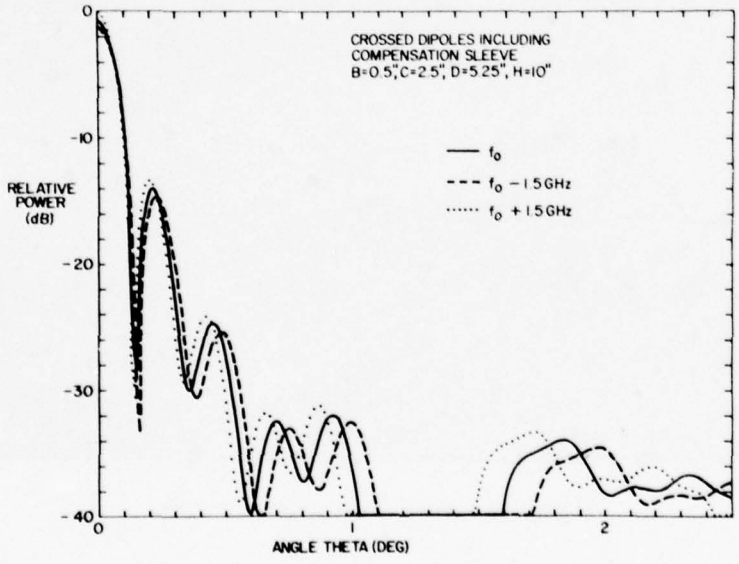

Figure 24. Radiation Patterns for the EHF Frequency Band

Table 3. Influence of the UHF Dipole on the EHF Boresight Gain of the Phase II UHF/EHF Hybrid Antenna (Calculated)

Condition	Gain (dB)
Cassegrain Antenna	REF
Solid Dipoles Added	-0.3
Solid Sleeve Added	-0.75

4.3 Gain and Radiation Pattern Measurements

The performance tests of the Phase II UHF/EHF Hybrid Antenna were undertaken in both frequency ranges for the two basic configurations with and without the UHF grid reflector. All EHF pattern measurements were again performed over the 1/2 mile range, using a right-hand circularly polarized 43.5 GHz signal. Gain level measurements were made by altering the EHF waveguide network on the Hybrid Antenna for linear reception and comparing the received levels against a standard gain horn (TRG Model B861). Some linear polarized patterns were also included. A short range of approximately 25 ft was used for measurement of UHF patterns and the determination of gain. Figure 25 shows a photograph of the UHF gain standard and test antenna. Patterns were recorded using linear polarization in the two major orthogonal planes. The equipment necessary for making circular polarized tests at UHF was not yet available, but RHCP operation can be predicted from the linear polarized results.

The initial EHF radiation patterns were reference plots of the Cassegrain antenna system in its optimized gain condition, without blockage for both the elevation and azimuth planes. These patterns, shown in Figures 26 and 27, are fairly symmetric and interference free except for a low level ground reflection at 12^{o} in the elevation plane. With the addition of the UHF dipole in front of the paraboloid, a new set of patterns were taken on an expanded scale for both right-hand circular and linear polarizations, and are compared with the reference patterns in Figures 28 through 31. The gain of the unblocked case was measured at 49.5 dB over an isotropic radiator and is reduced by 0.8 dB when the UHF dipole is added. The gain figures are detailed in Figure 30. Additional pattern changes are noted with the increase in sidelobe levels and the slight narrowing of the main beam. The sidelobe increase is not severe, and the resulting levels seem quite reasonable for the present application. Of primary importance is that the small (0.8 dB) gain reduction emphasizes that incorporating the UHF dipole imposes only a very minor penalty to the EHF communication link.

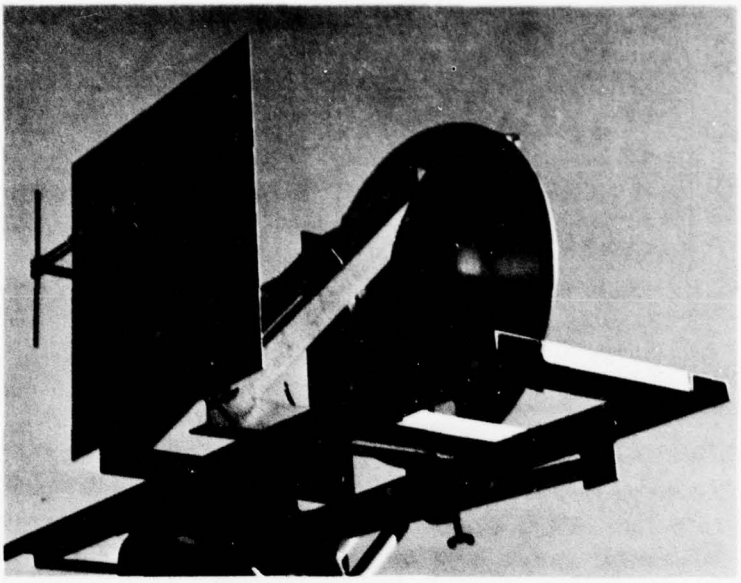

Figure 25. UHF Gain Standard

A complete set of UHF patterns over the 225 to 400 MHz band are presented in Figures 32 to 53. The UHF grid reflector was then installed in the paraboloid, and a second set of UHF patterns were recorded in Figures 54 through 75. The corresponding gain measurements for both cases over the upper portion of this frequency range are summarized in Table 4.

Table 4. Measured UHF Gain of the Phase II Hybrid Antenna

Frequency (MHz)	Gain (dBi)	
	Without Grid Refl.	With Grid Refl.
400	8.5	9.7
380	8.4	9.9
360	10.0	9.4
340	9.7	8.8
320	7.5	6.7

No gain measurements were made below 320 MHz. In general, the UHF patterns have good characteristics above 320 MHz for both UHF configurations. However, at 320 MHz and below, the E- and H-plane pattern shapes become extremely dissimilar and would have a definite affect on off-axis CP operation. On the other hand, the axial gain at UHF is significantly better than the fixed fuselage antenna.

Additional EHF pattern and gain measurements were required by the installation of the UHF grid reflector. These measurements showed that adding the grid reduced the EHF gain as referred to the unblocked antenna by 3.2 dB. Table 5 lists all the EHF gain figures for comparison.

Table 5. Measured EHF Gain of the Phase II Hybrid Antenna

Condition	Gain (dBi)
Cassegrain Antenna	49.5
UHF Dipole Installed	48.7
UHF Grid Reflector Installed	46.3

The radiation patterns with the reflector grid installed are plotted in Figures 76 and 77.

Since the grid introduced such a substantial loss of EHF gain and did not markedly improve the UHF performance except at certain points in the frequency band, it was determined that the grid should be omitted from further design study.

4.4 Fuselage Simulation Measurements

The Phase II Hybrid Antenna combines a UHF capability in an EHF paraboloidal reflector, as a means of increasing the UHF performance over that which is presently used in contemporary aircraft. When a reflector antenna of these dimensions is operated at microwave frequencies and is directed toward the horizon or near-horizon, some minor variations in the pattern shape and boresight gain due to reflections from the aircraft's fuselage will be observed. In the microwave frequency region, these changes are small and can be tolerated. However, with UHF operation, these fuselage reflections are more significant because of the relatively small reflector size. An experiment was conducted to estimate the severity of these effects for a worst case geometry.

An experimental method to test the fuselage effects at UHF was implemented by constructing a 4 ft × 4 ft ground screen and mounting it 3 in. from the edge of the Hybrid Antenna and parallel to its axis. Figures 78 through 83 provide a sketch of the experimental fuselage simulation set up and some radiation pattern data under its influence. It may be seen that the ground screen extends forward of the antenna aperture by approximately 3.5 ft and is pivoted at a point in line with the antenna aperture. Superimposed patterns for both the E- and H-plane orientations over various aspect angles, α_F, have been recorded at three frequencies. Extensive pattern reshaping takes place as the aspect angle is varied and the UHF boresight gain does increase and decrease by a few decibels.

The key feature of these data is that although substantial pattern degradation results from placing a reflecting sheet in the immediate vicinity of the antenna, the minimum boresight gain is still in excess of 6 dB over the frequency range tested, which is a major improvement over the present stationary UHF antenna. In addition, the actual aircraft should have a smaller specular reflection component because of its convex surface, and so the present experimental results should be nearly "worst case" data.

5. CONCLUSIONS

The results of this experimental development program indicate that the performance specifications of efficient EHF and UHF communications systems can be met by installing a UHF dipole in the radiating aperture of an EHF paraboloid. The objective was to increase the UHF gain over the 0 dB of present antenna systems while preserving the EHF operational capability. These fundamental experimental tests indicate an approximate gain level of 6 dBi can be achieved over the UHF operating band. The EHF gain is reduced by 0.8 dB while the corresponding radiation patterns are degraded only slightly. This substantial increase in UHF gain makes the EHF/UHF option extremely attractive from a link-margin point of view.

Several unanswered questions should be addressed if future work on this problem seems warranted by operational requirements. The effects of the aircraft environment has been examined by a very basic experiment. Further assessment should require that the gain and pattern measurements be performed with the antenna installed on an aircraft platform including the radome. It is expected that the UHF gain might be slightly higher for the real application. Although no circularly polarized measurements were performed at UHF, the orthogonal linearly polarized patterns of this report indicate that a circularly polarized wave would suffer some pattern deterioration off the boresight axis. Specifically, if one examines the UHF patterns throughout the frequency band (Figures 32 to 53), the

E- and H-plane patterns are fairly symmetric but quite dissimilar in shape. CP operation at each frequency would correspondingly yield a high axial ratio at angles off boresight. If, however, the aircraft application uses the EHF band or the ephemeris data for antenna pointing, the UHF link will always be operated on boresight or beam maximum where the off axis ratio will be of little concern.

In addition, the paraboloid strut support causes some pattern deterioration at the UHF band, but these effects have been minimized by locating the dipoles at angles between the struts so that the beam shape for the various polarizations remains symmetric.

Another consideration not addressed in this study is the power handling capability of the UHF dipole. The grid sleeve has been relocated for the Phase II antenna, which in turn results in some changes to the impedance match. Any further development should include additional dipole optimization to meet specific input power level and VSWR requirements. In addition, the rather extended balun section of the dipole should also be shortened or folded during this study so that mechanical interference with the radome surface does not affect antenna pointing. These issues have not been addressed in the current program, but they do not present serious design problems and, in our opinion, are minor development efforts that can be addressed when and if the Air Force elects to develop a UHF/EHF SATCOM system.

Assuming that the power loss budget achieved by this antenna structure at both frequency bands is satisfactory, the data provided would indicate that combining a UHF dipole in the aperture of an EHF paraboloid presents an extremely attractive alternative to the use of an omnidirectional UHF and directional EHF antenna. The overall conclusion of this study is that this enhanced UHF performance can be achieved with minimal additional design effort and without major design compromises at EHF.

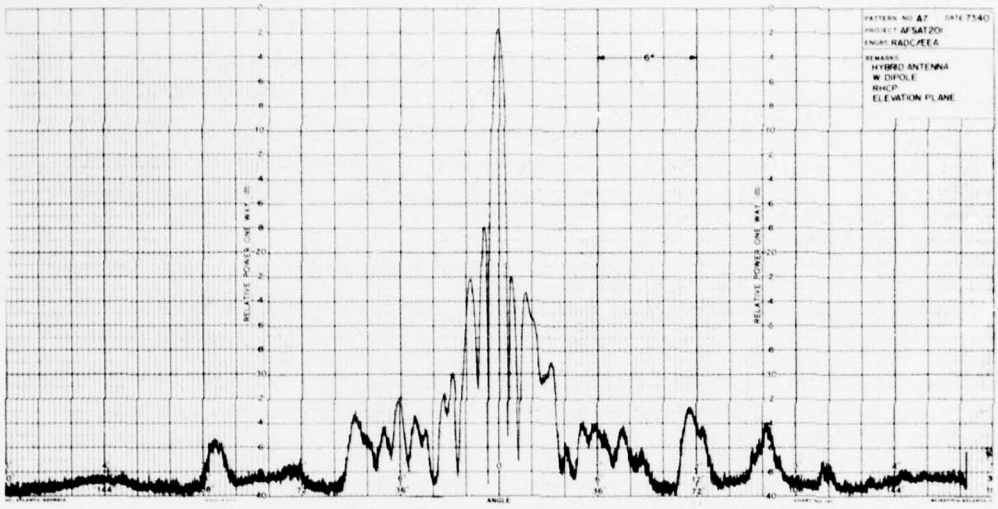

Figure 26. EHF Radiation Pattern in Elevation Plane Without the UHF Dipole

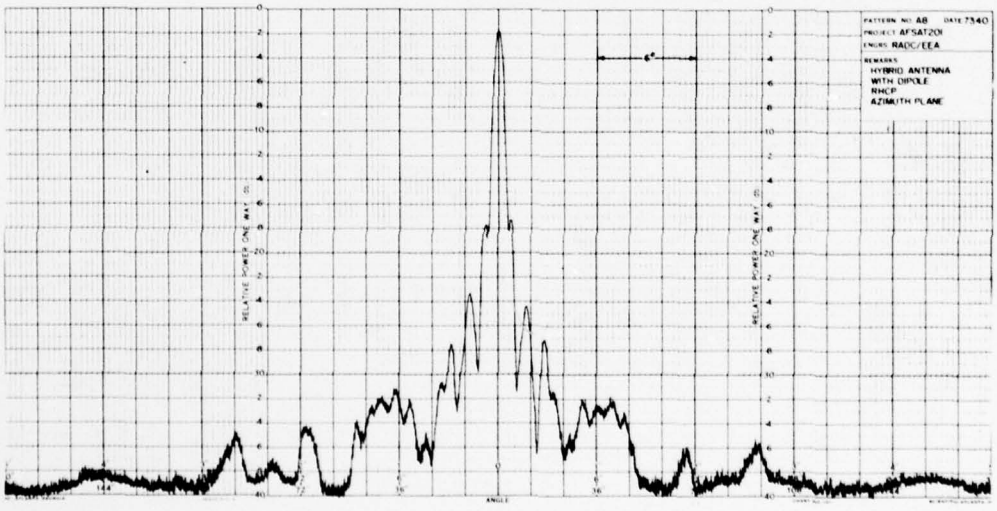

Figure 27. EHF Radiation Pattern in Azimuth Plane Without the UHF Dipole

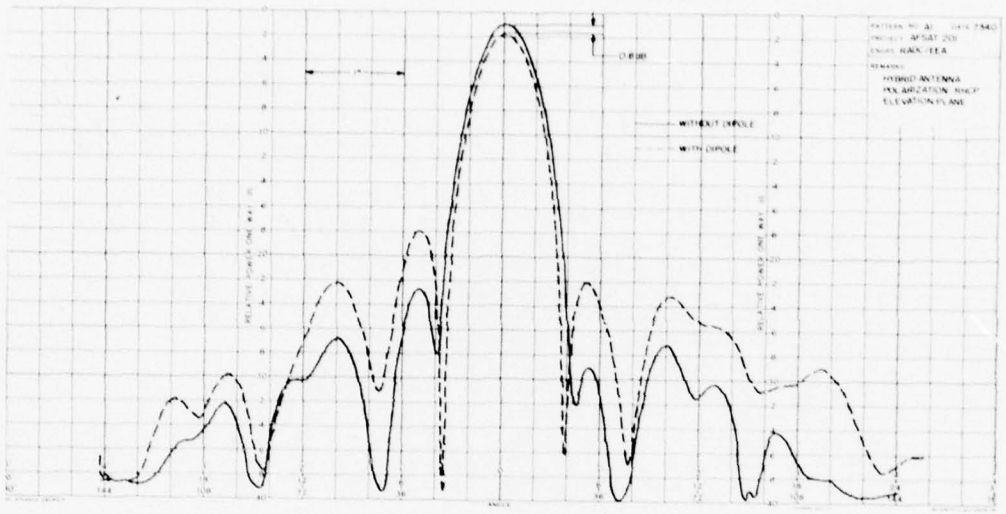

Figure 28. EHF Radiation Patterns With UHF Dipole in Elevation Plane

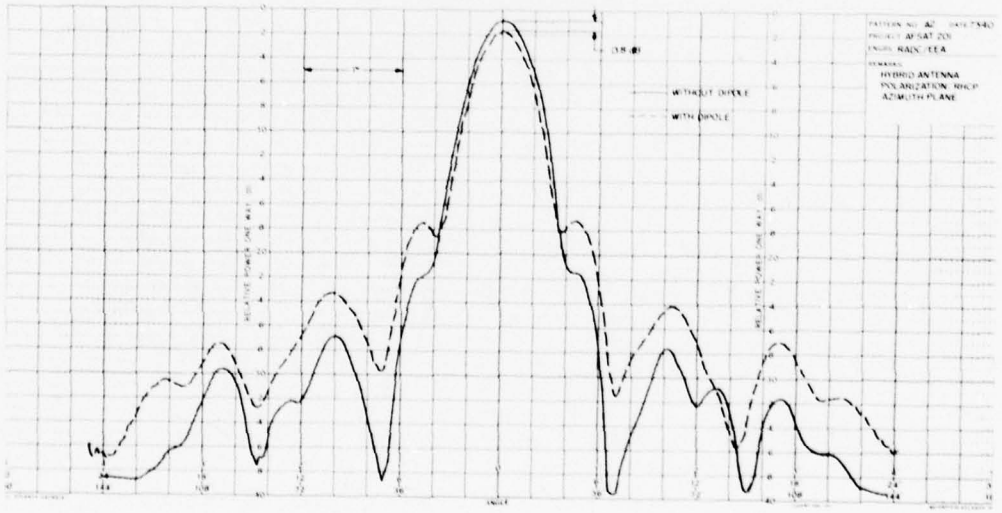

Figure 29. EHF Radiation Patterns With UHF Dipole in Azimuth Plane

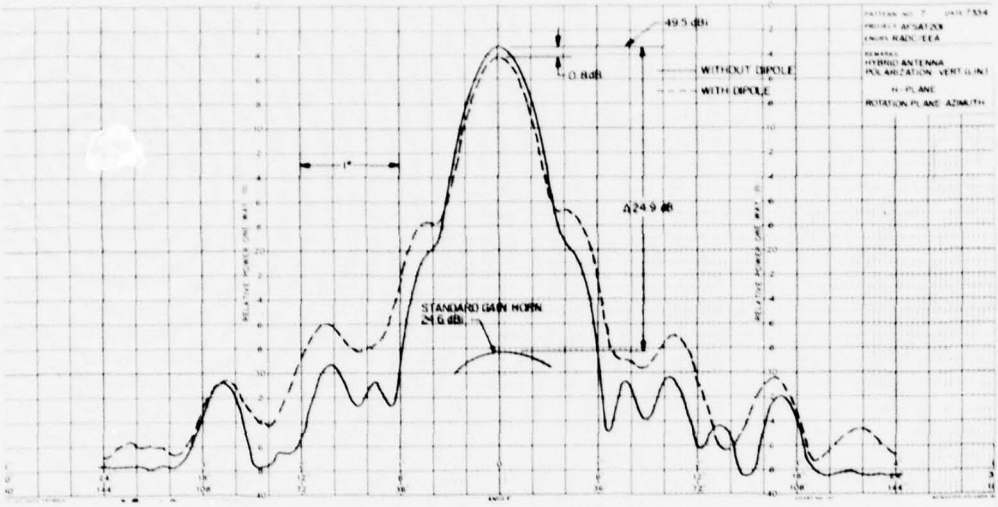

Figure 30. EHF Radiation Patterns With UHF Dipole (Linear Polarization, H-Plane)

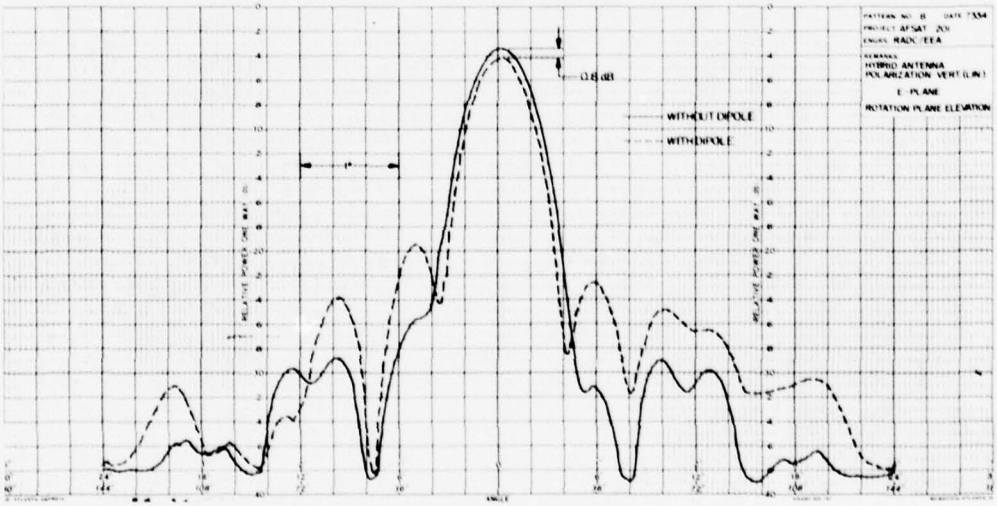

Figure 31. EHF Radiation Patterns With UHF Dipole (Linear Polarization, E-Plane)

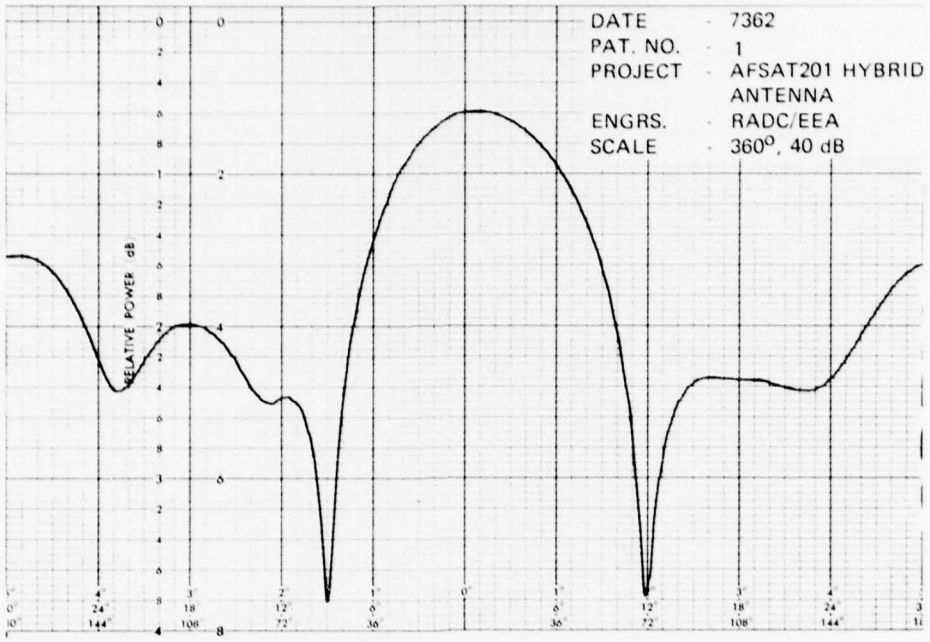

Figure 32. UHF Radiation Pattern (E-Plane, 225 MHz)

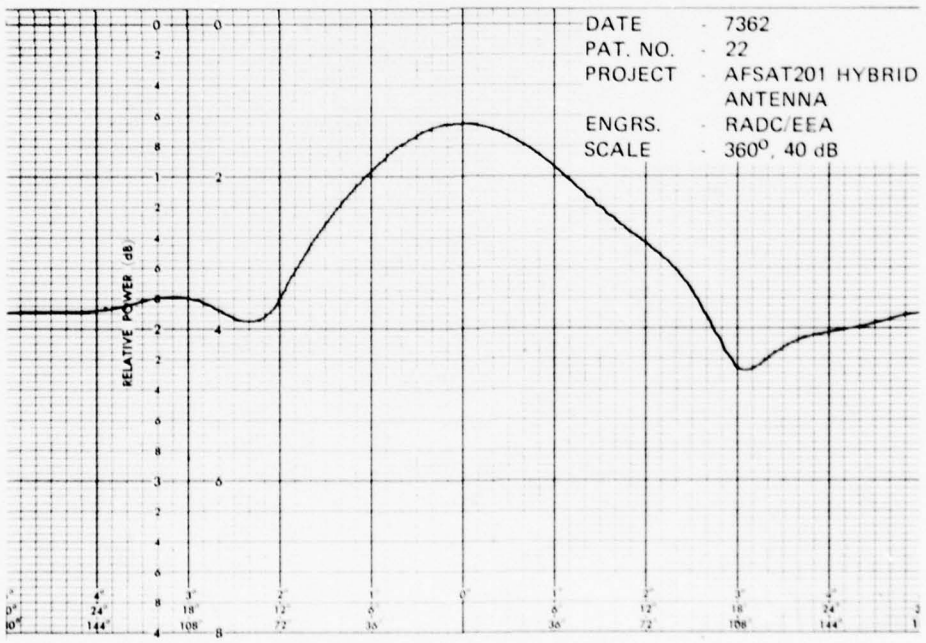

Figure 33. UHF Radiation Pattern (H-Plane, 225 MHz)

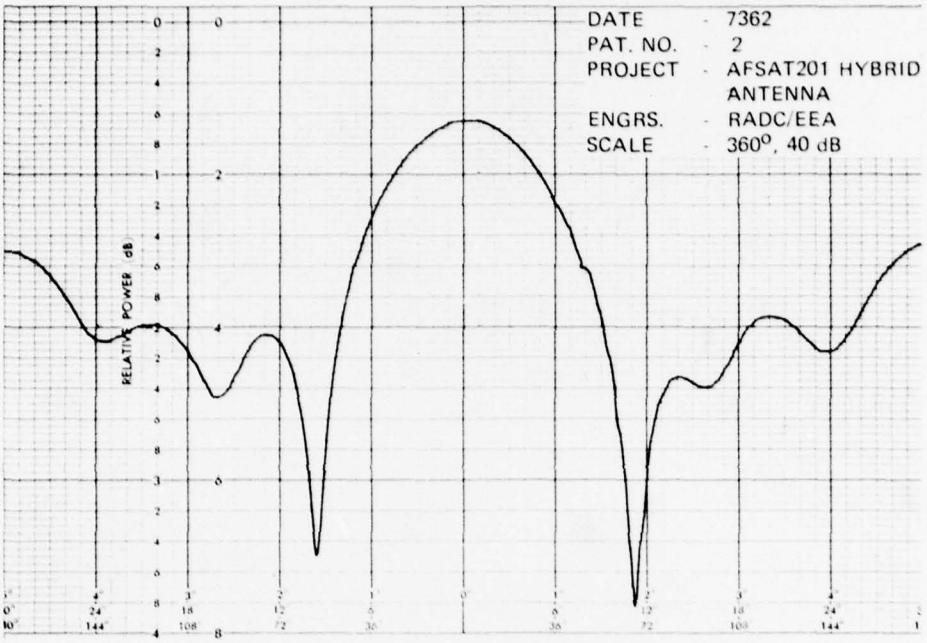

Figure 34. UHF Radiation Pattern (E-Plane, 240 MHz)

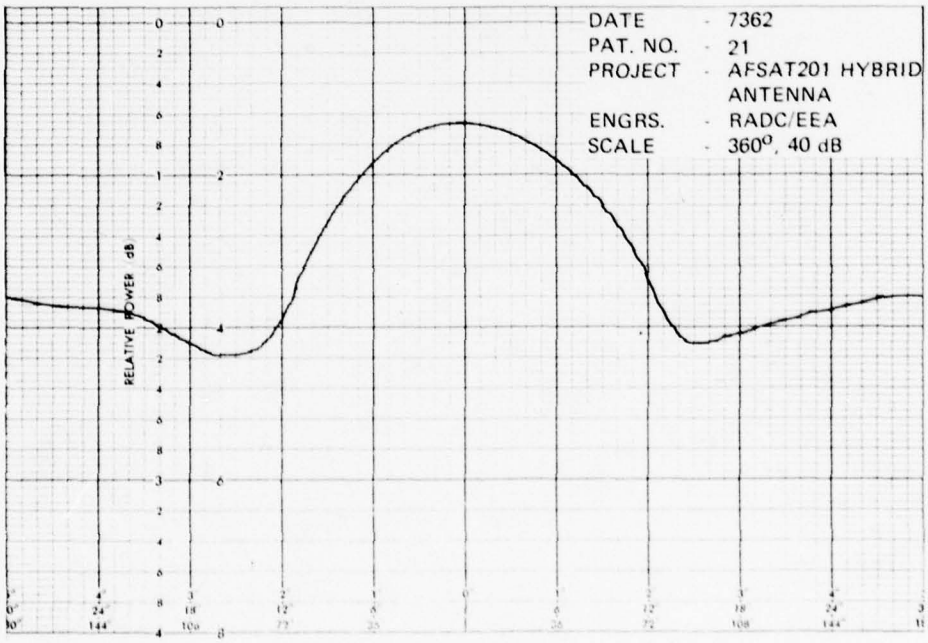

Figure 35. UHF Radiation Pattern (H-Plane, 240 MHz)

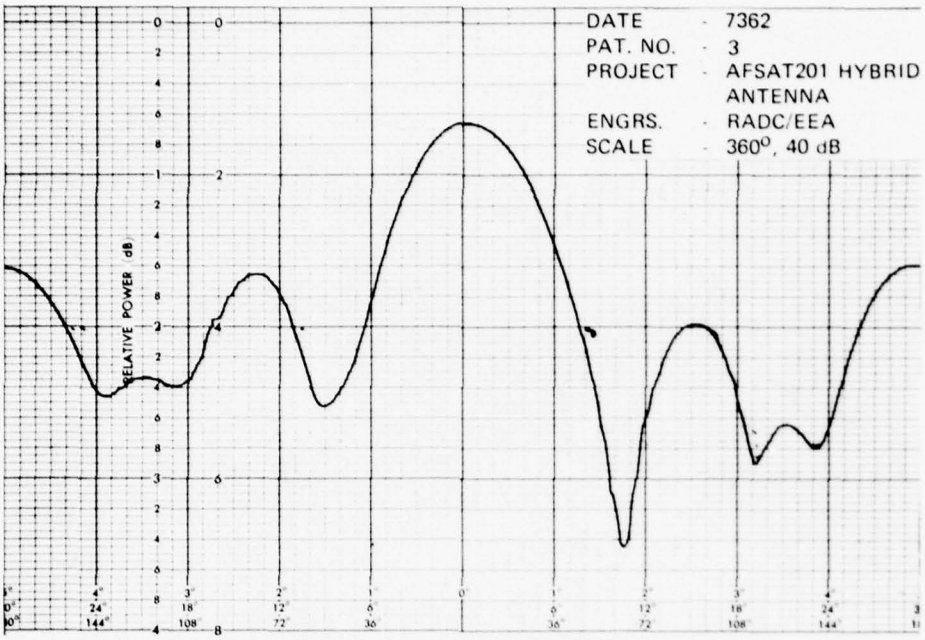

Figure 36. UHF Radiation Pattern (E-Plane, 260 MHz)

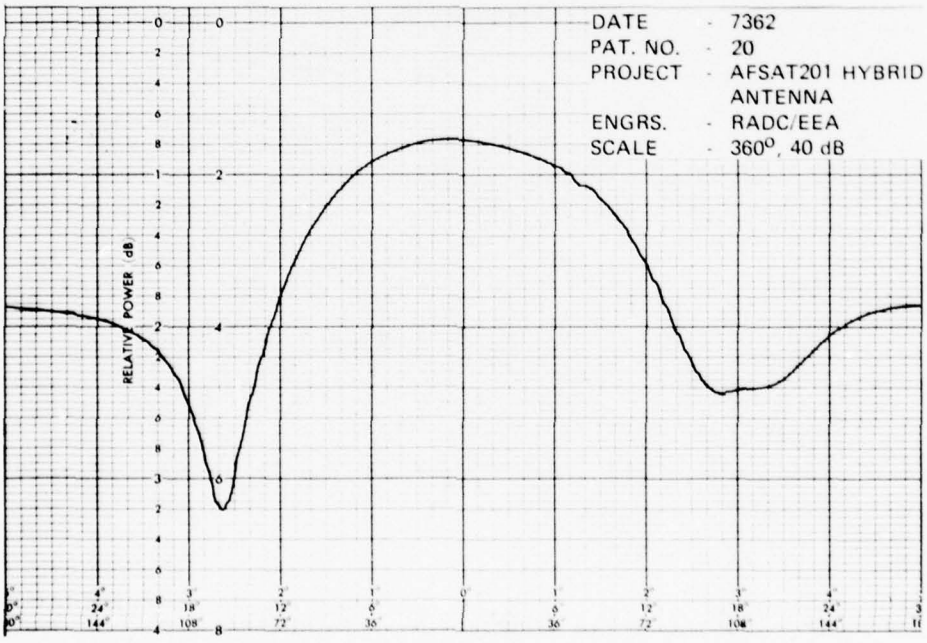

Figure 37. UHF Radiation Pattern (H-Plane, 260 MHz)

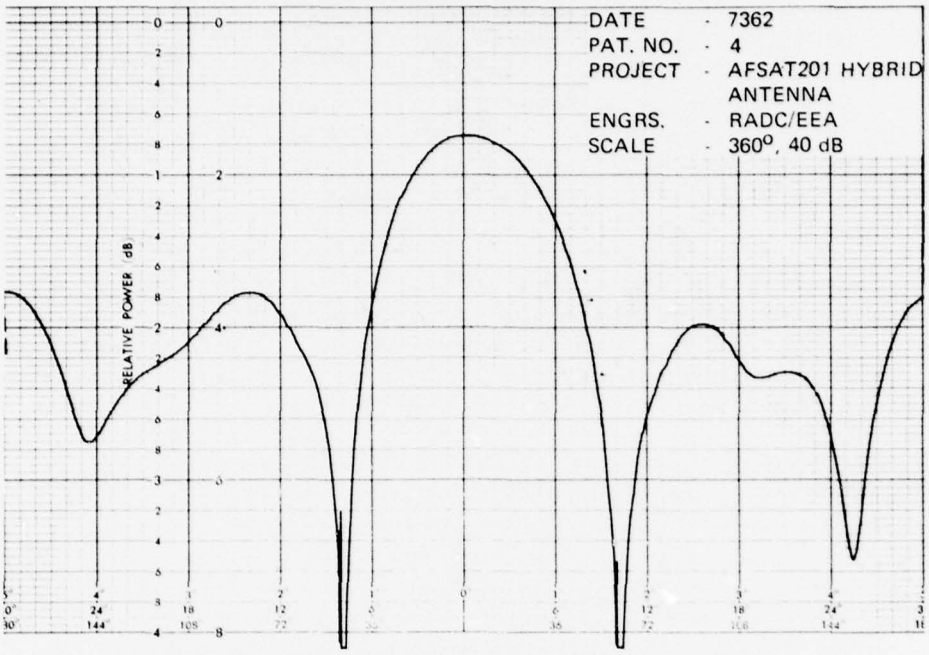

Figure 38. UHF Radiation Pattern (E-Plane, 280 MHz)

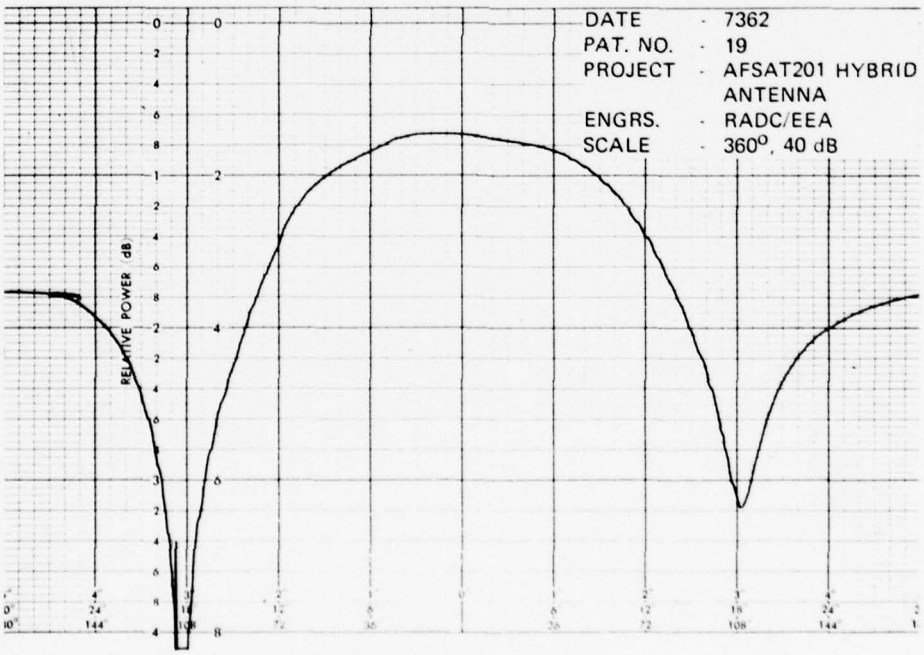

Figure 39. UHF Radiation Pattern (H-Plane, 280 MHz)

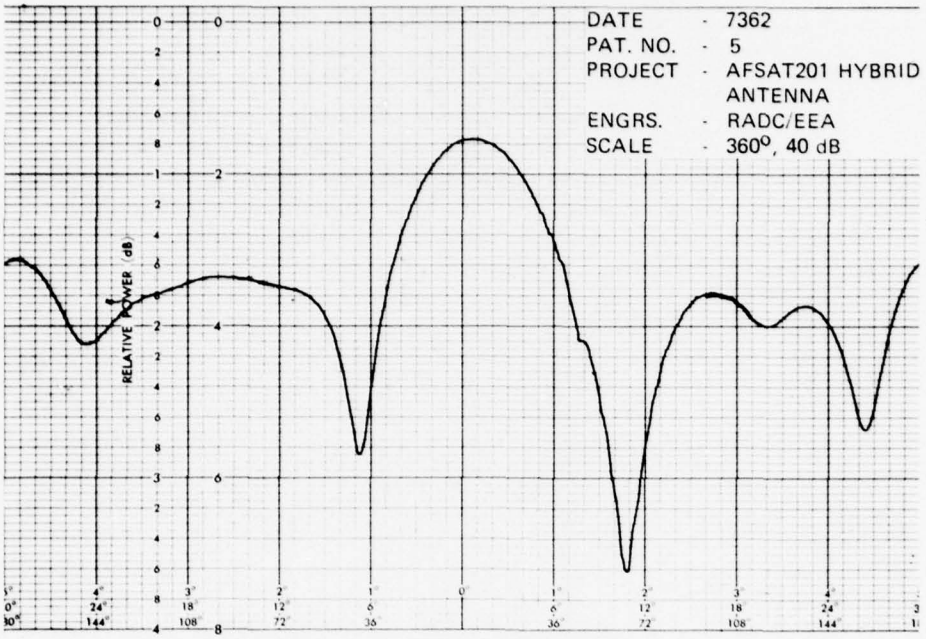

Figure 40. UHF Radiation Pattern (E-Plane, 293 MHz)

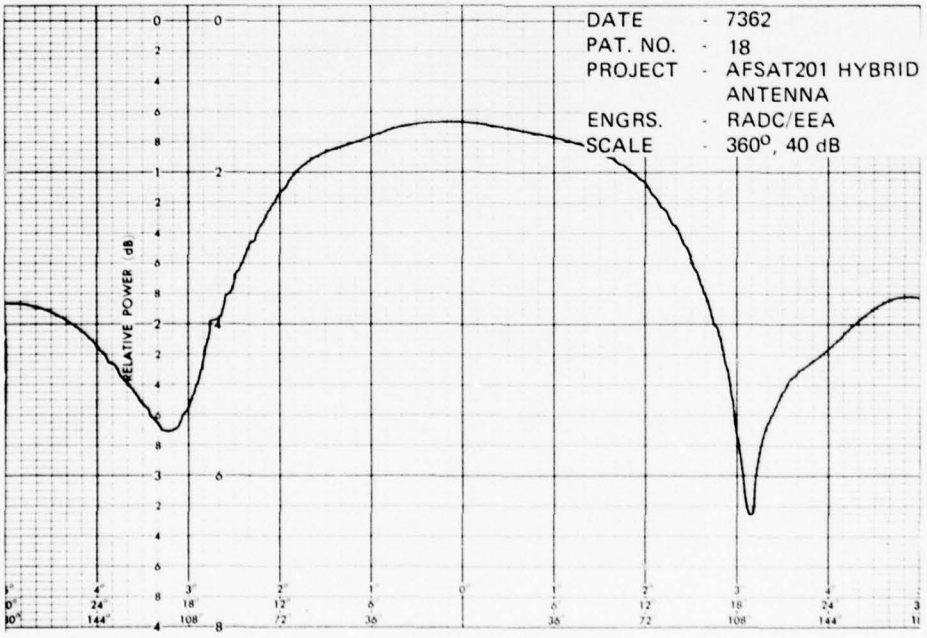

Figure 41. UHF Radiation Pattern (H-Plane, 293 MHz)

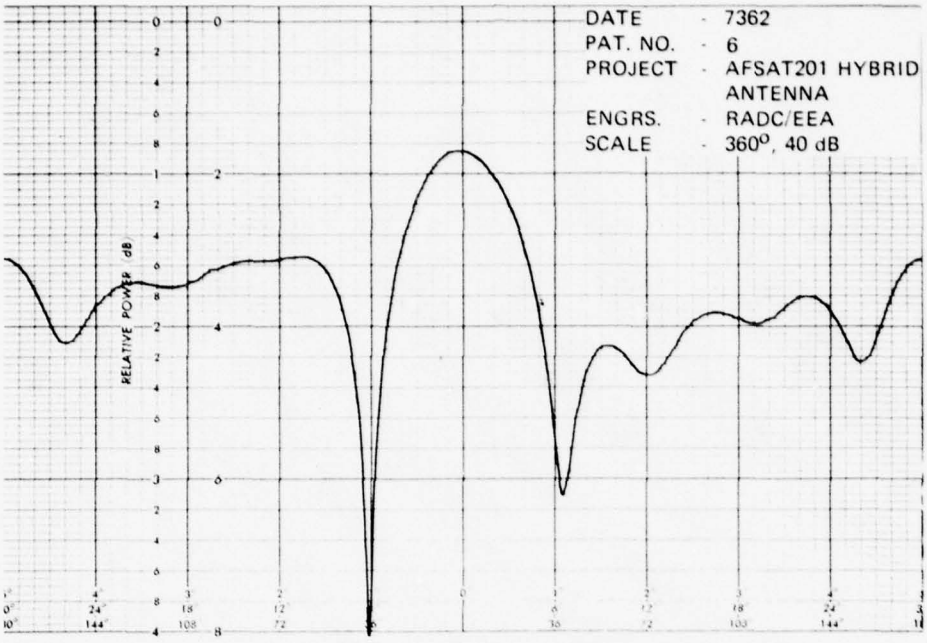

Figure 42. UHF Radiation Pattern (E-Plane, 300 MHz)

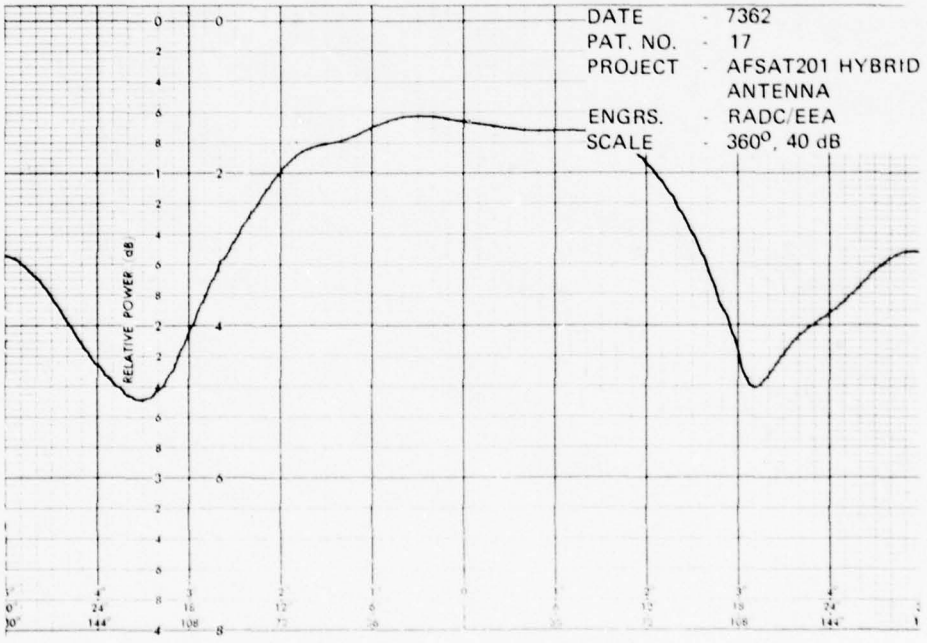

Figure 43. UHF Radiation Pattern (H-Plane, 300 MHz)

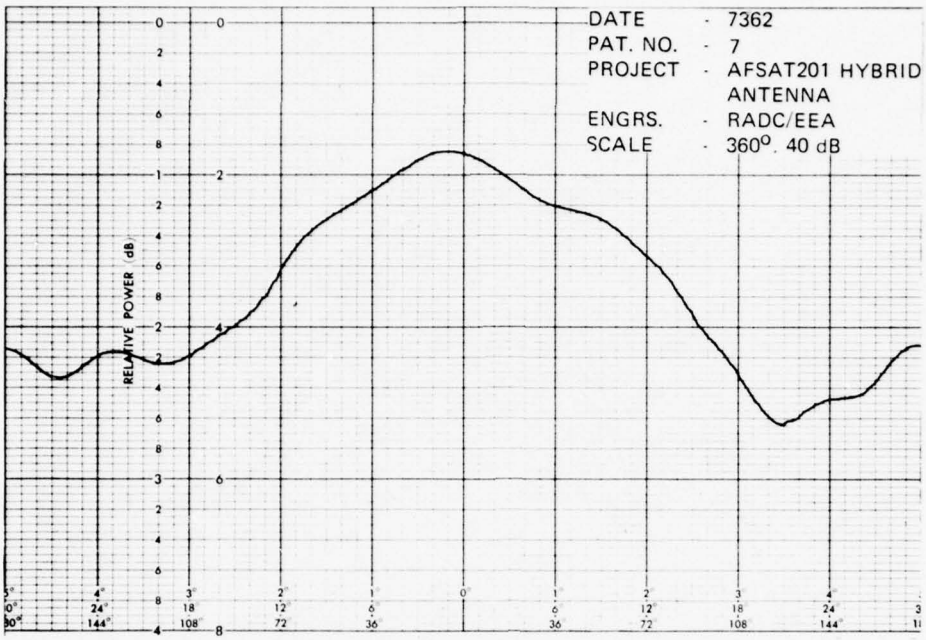

Figure 44. UHF Radiation Pattern (E-Plane, 320 MHz)

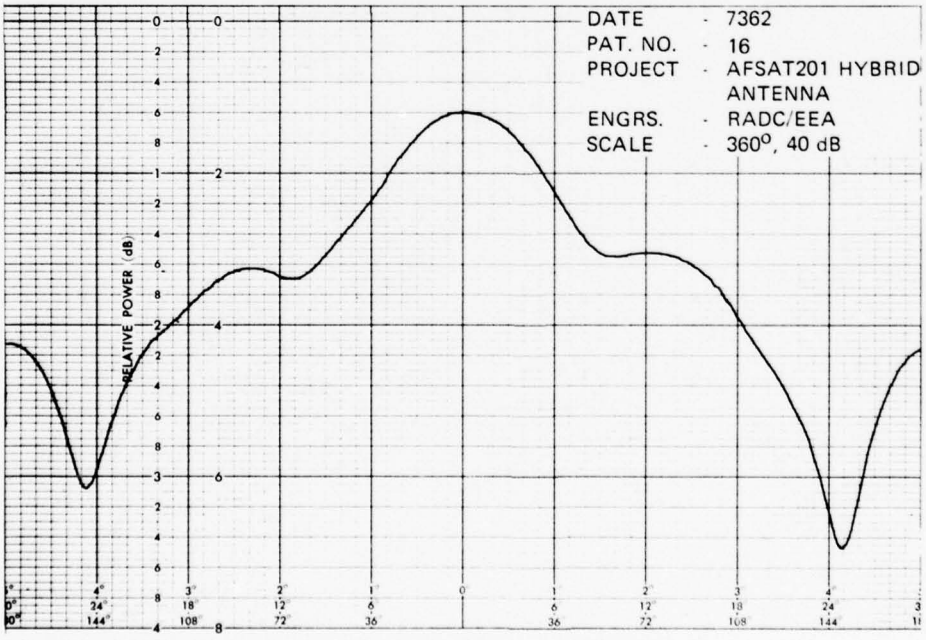

Figure 45. UHF Radiation Pattern (H-Plane, 320 MHz)

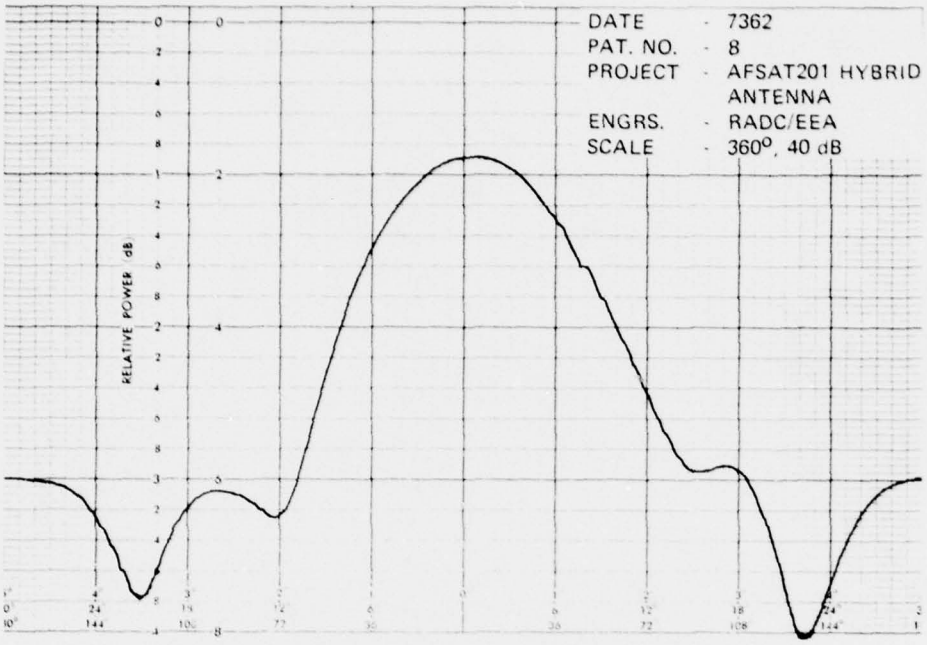

Figure 46. UHF Radiation Pattern (E-Plane, 340 MHz)

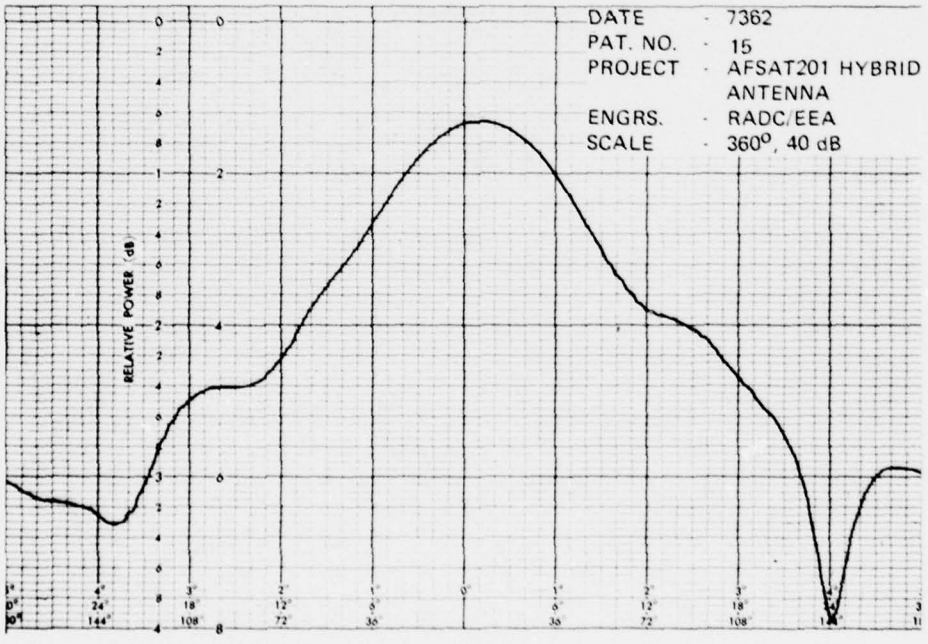

Figure 47. UHF Radiation Pattern (H-Plane, 340 MHz)

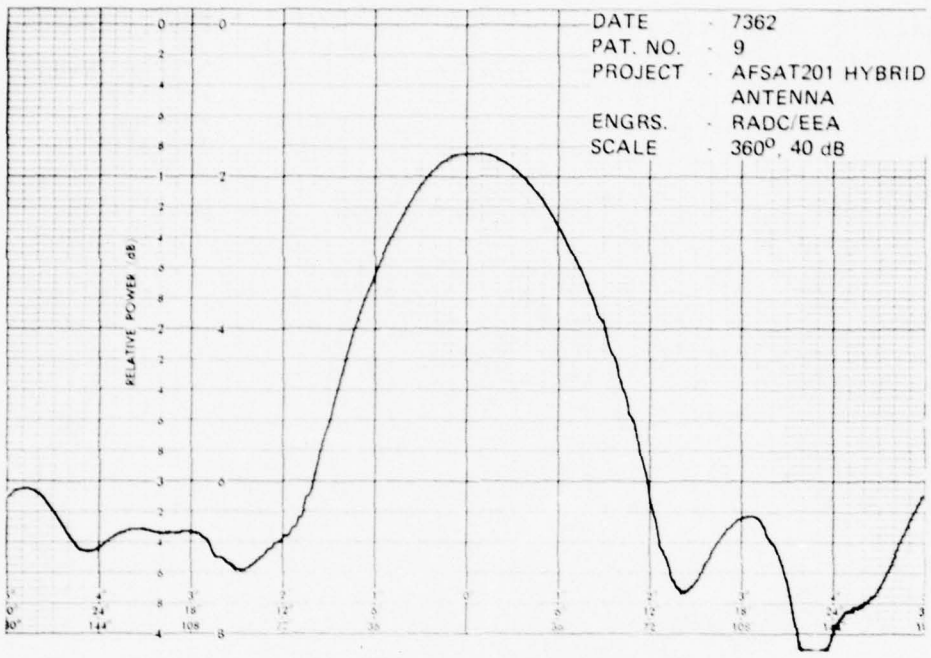

Figure 48. UHF Radiation Pattern (E-Plane, 360 MHz)

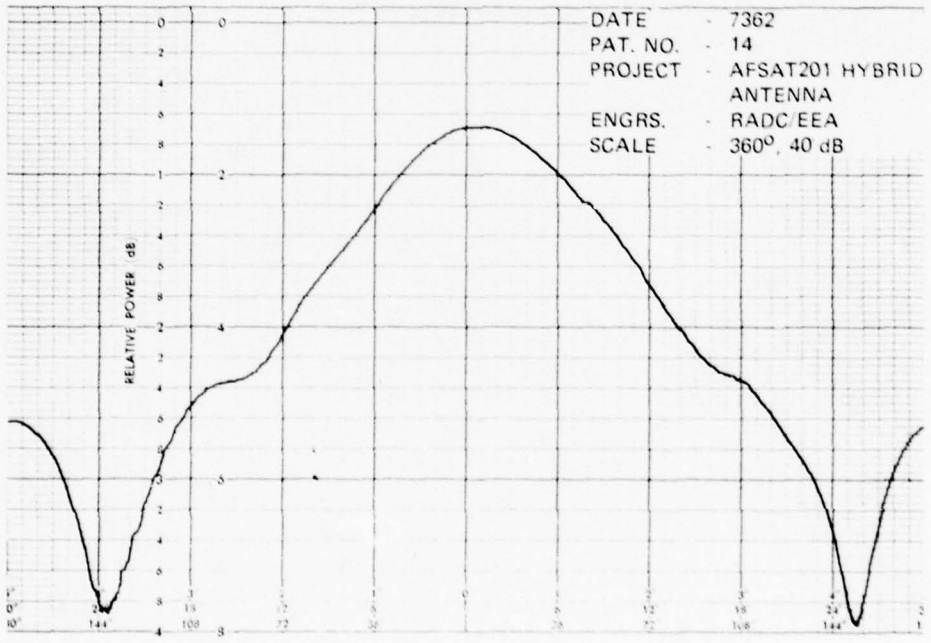

Figure 49. UHF Radiation Pattern (H-Plane, 360 MHz)

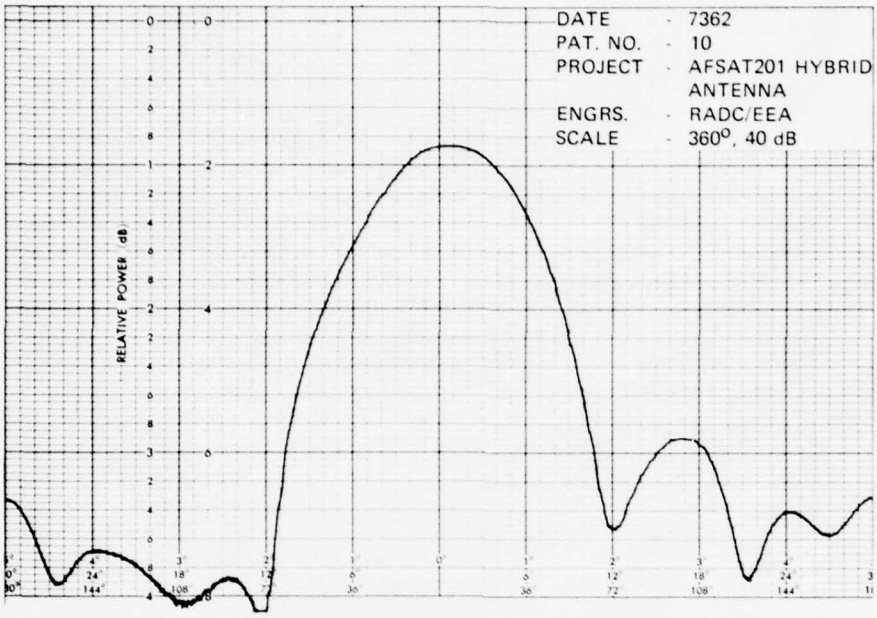

Figure 50. UHF Radiation Pattern (E-Plane, 380 MHz)

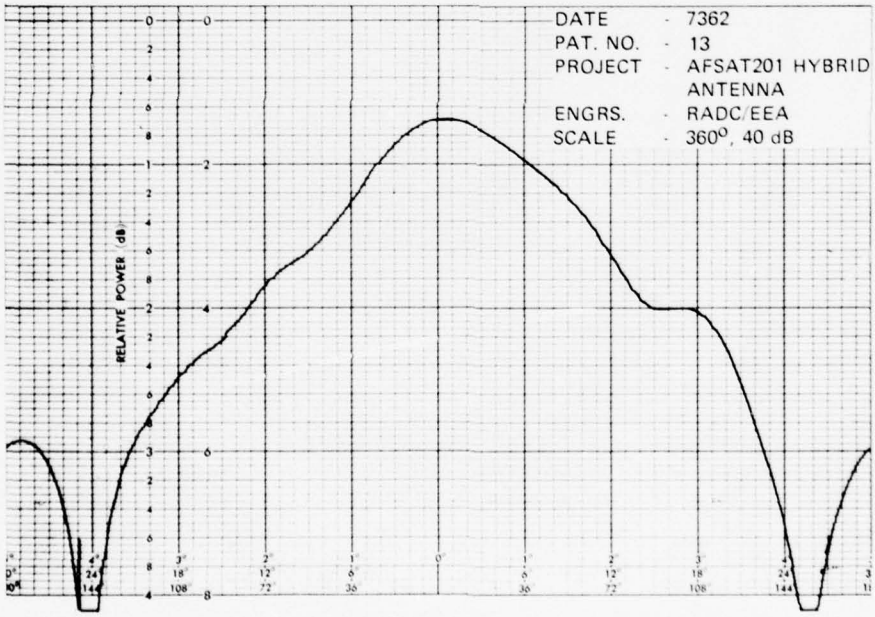

Figure 51. UHF Radiation Pattern (H-Plane, 380 MHz)

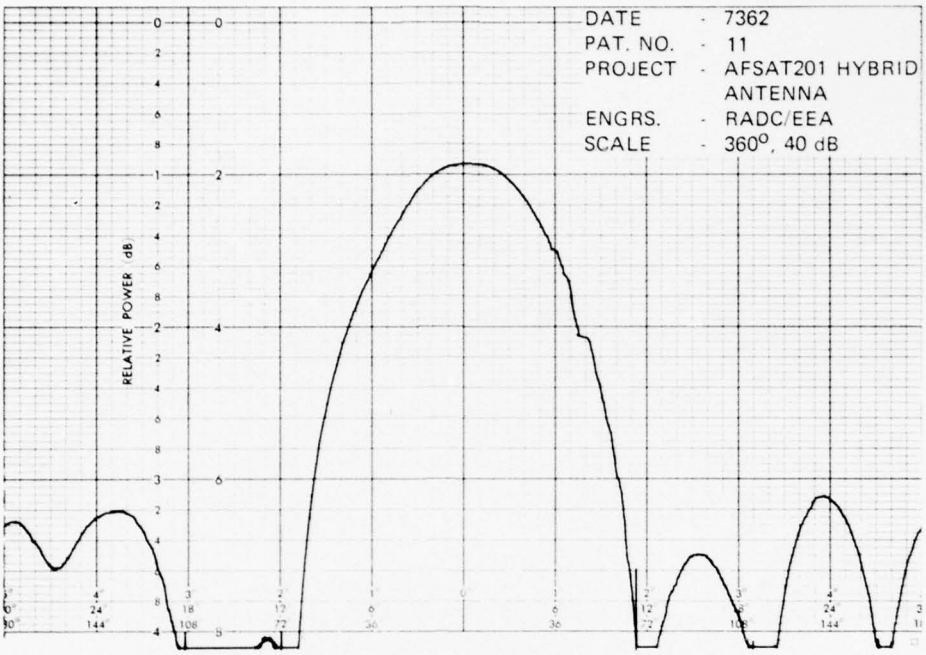

Figure 52. UHF Radiation Pattern (E-Plane, 400 MHz)

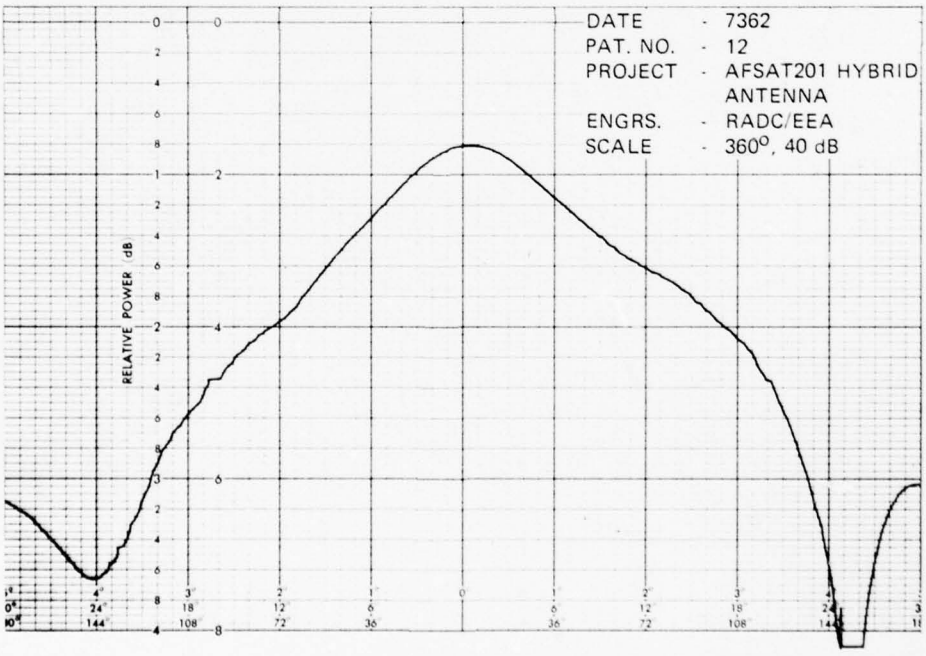

Figure 53. UHF Radiation Pattern (H-Plane, 400 MHz)

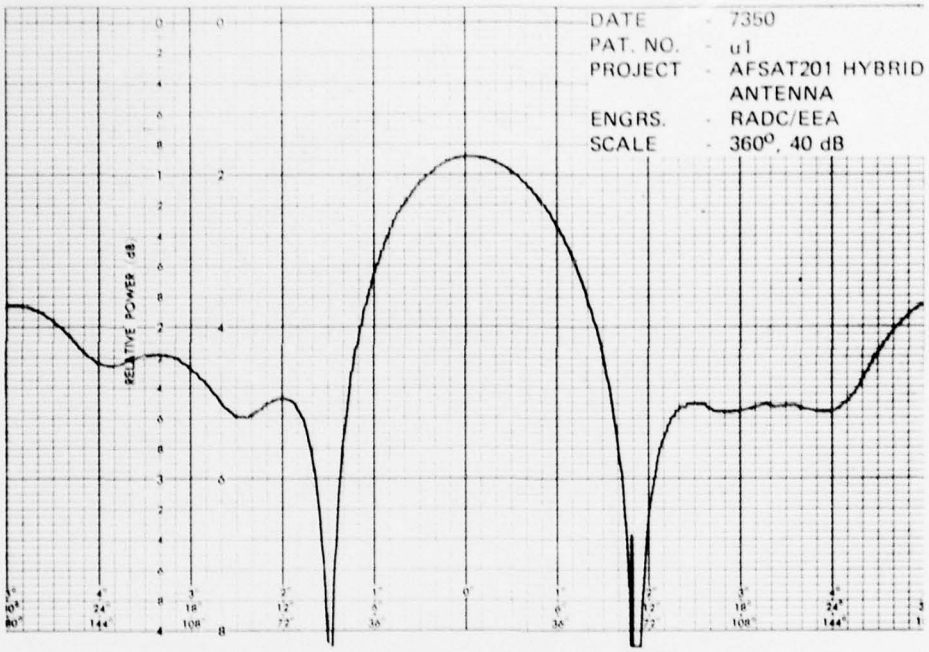

Figure 54. UHF Radiation Pattern with Grid Reflector (E-Plane, 225 MHz)

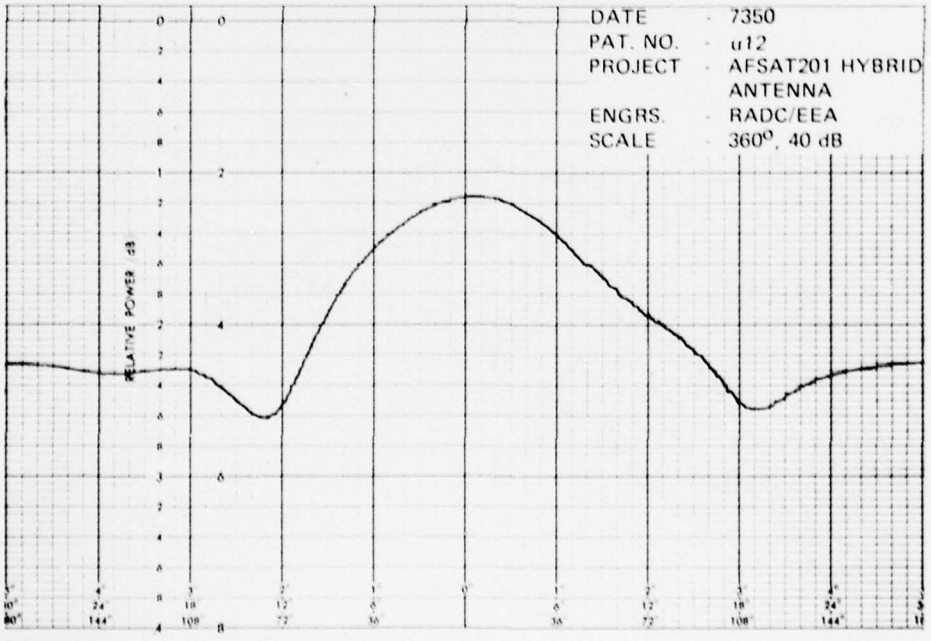

Figure 55. UHF Radiation Pattern With Grid Reflector (H-Plane, 225 MHz)

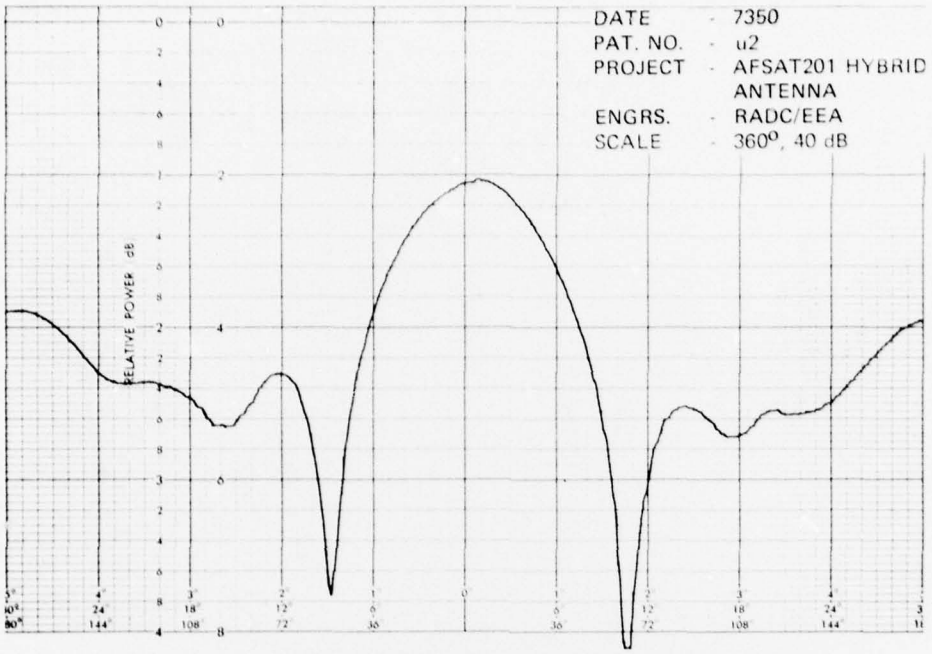

Figure 56. UHF Radiation Pattern With Grid Reflector (E-Plane, 240 MHz)

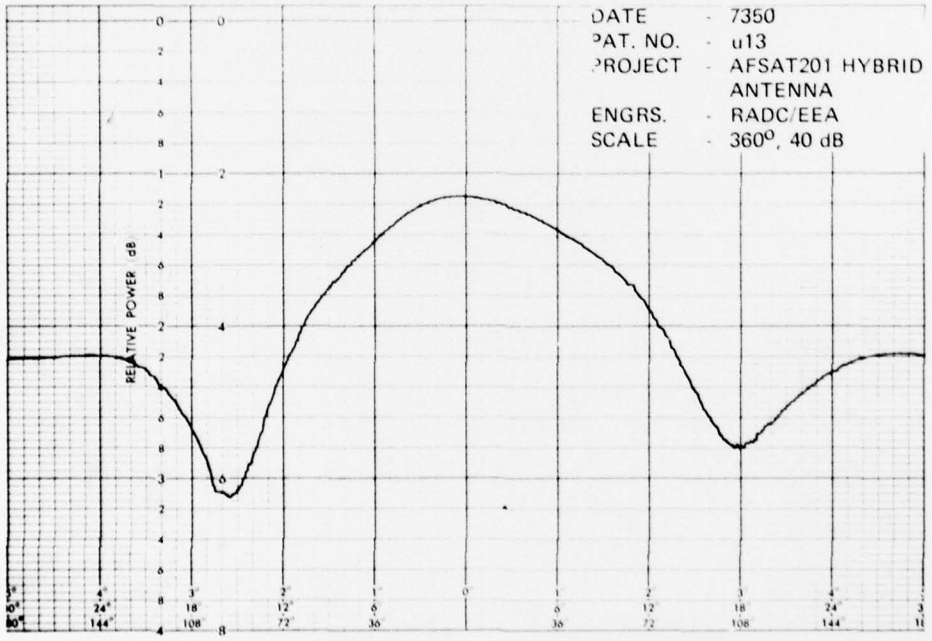

Figure 57. UHF Radiation Pattern With Grid Reflector (H-Plane, 240 MHz)

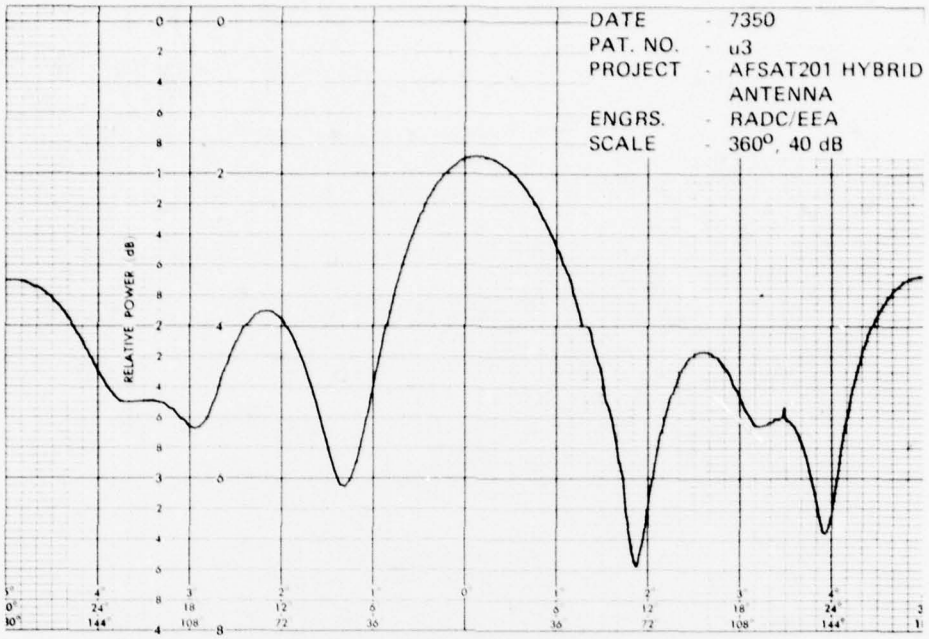

Figure 58. UHF Radiation Pattern With Grid Reflector (E-Plane, 260 MHz)

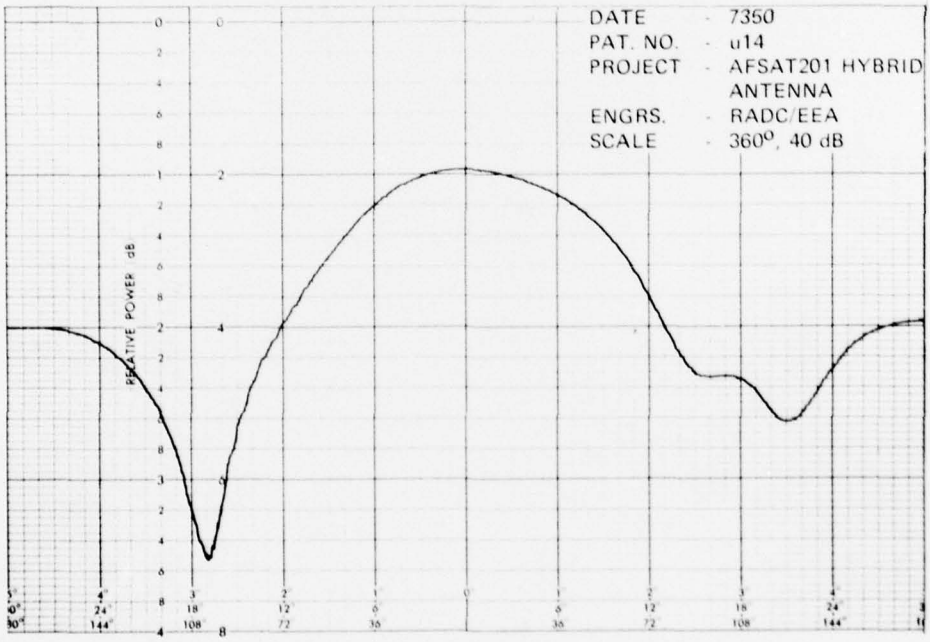

Figure 59. UHF Radiation Pattern With Grid Reflector (H-Plane, 260 MHz)

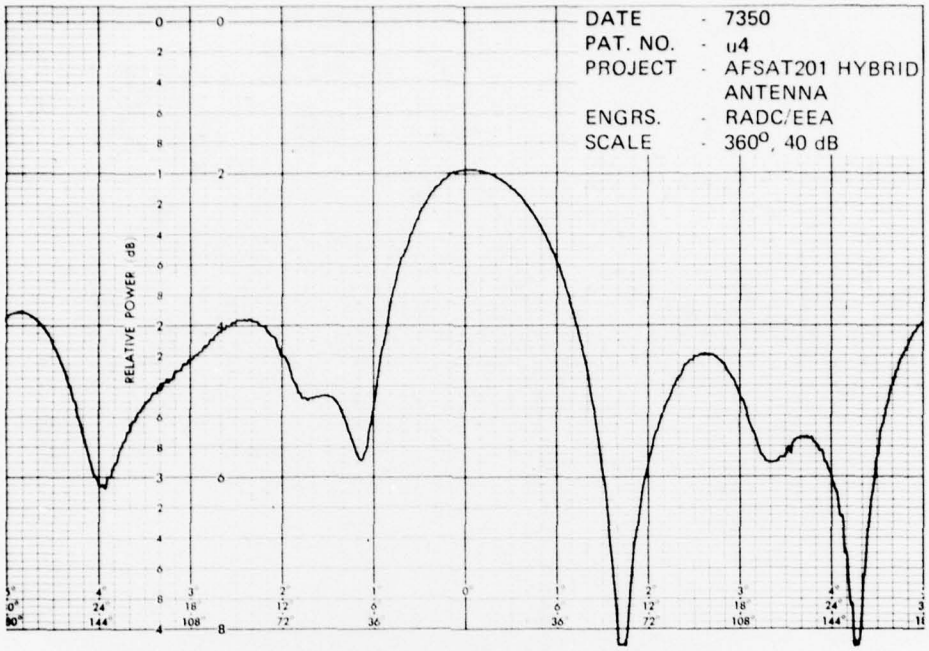

Figure 60. UHF Radiation Pattern With Grid Reflector (E-Plane, 280 MHz)

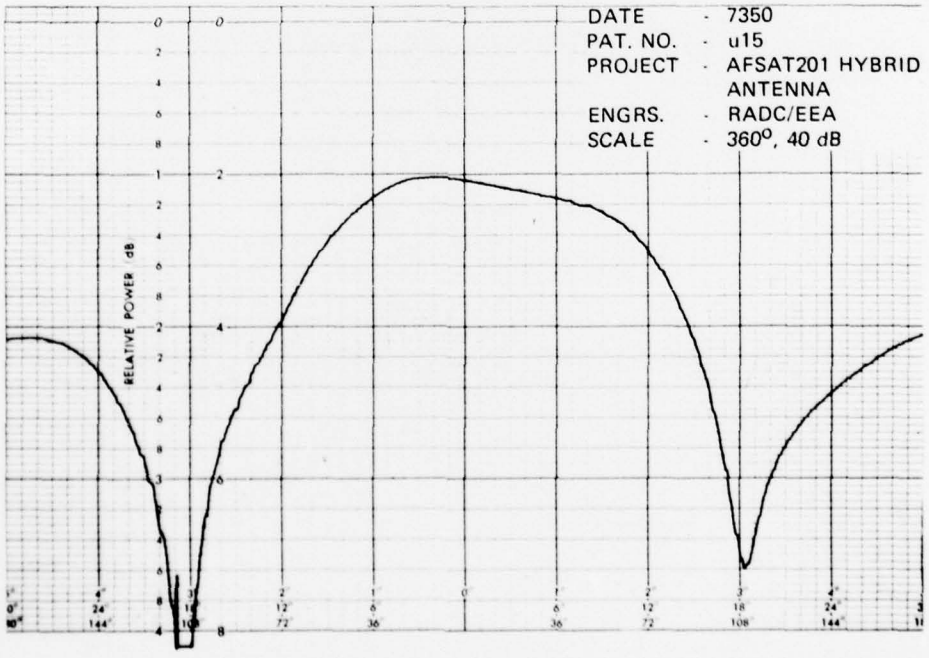

Figure 61. UHF Radiation Pattern With Grid Reflector (H-Plane, 280 MHz)

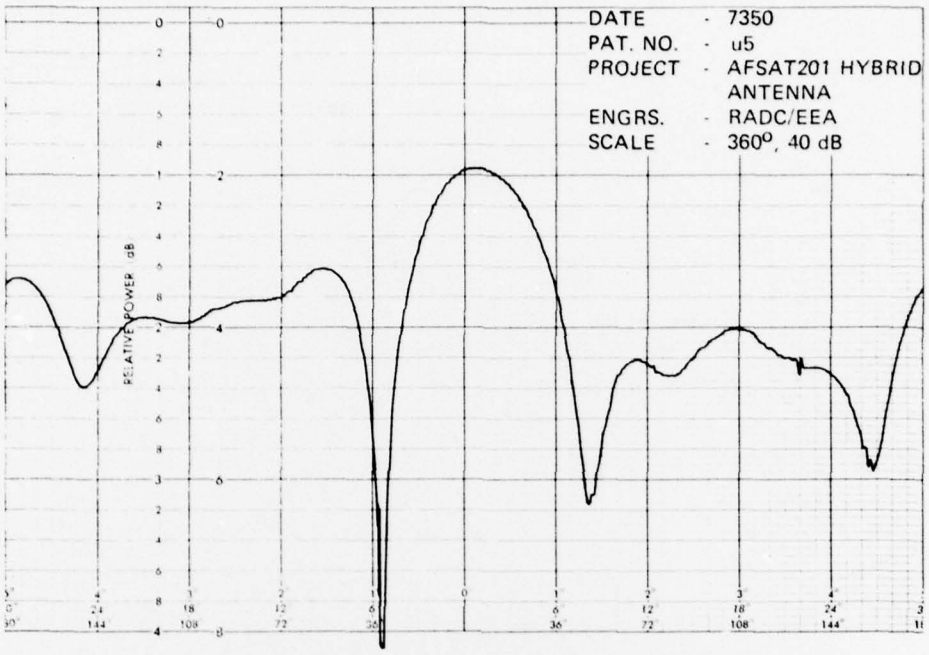

Figure 62. UHF Radiation Pattern With Grid Reflector (E-Plane, 293 MHz)

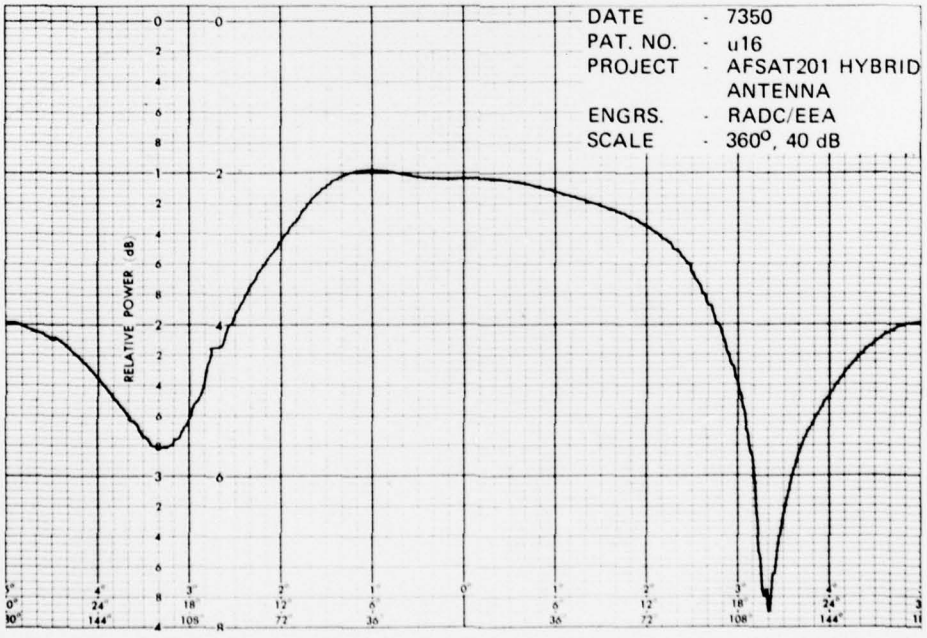

Figure 63. UHF Radiation Pattern With Grid Reflector (H-Plane, 293 MHz)

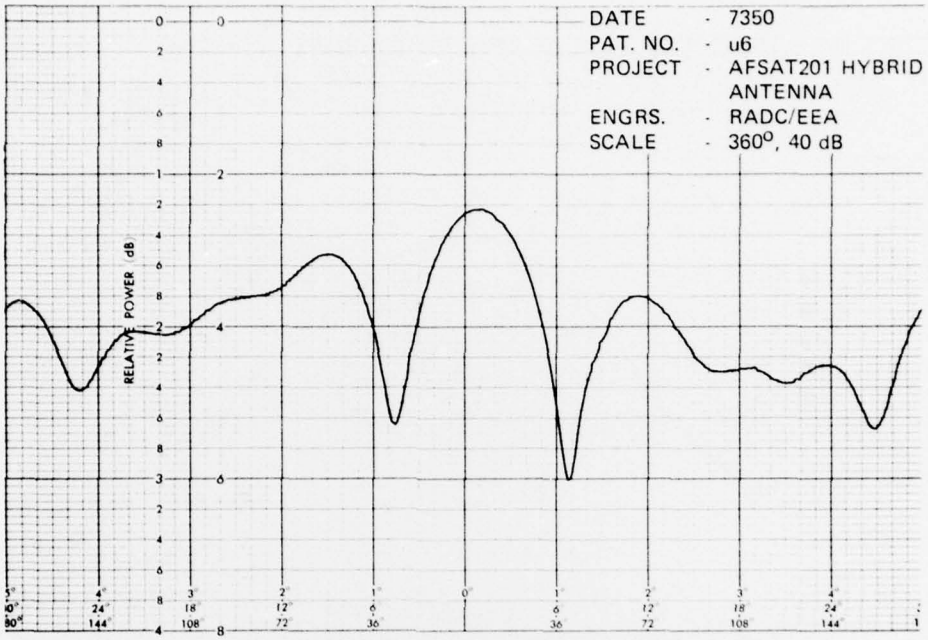

Figure 64. UHF Radiation Pattern With Grid Reflector (E-Plane, 300 MHz)

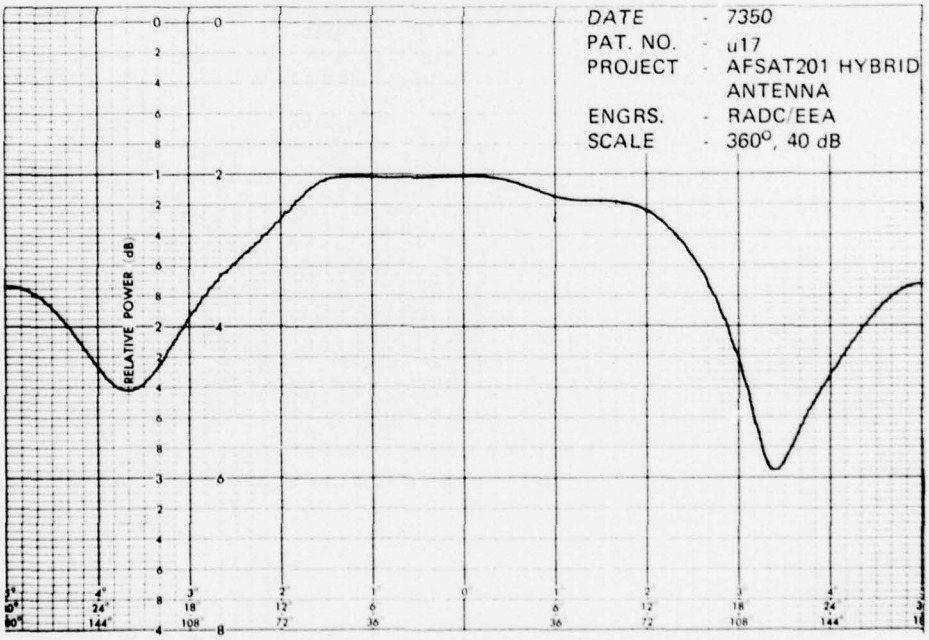

Figure 65. UHF Radiation Pattern With Grid Reflector (H-Plane, 300 MHz)

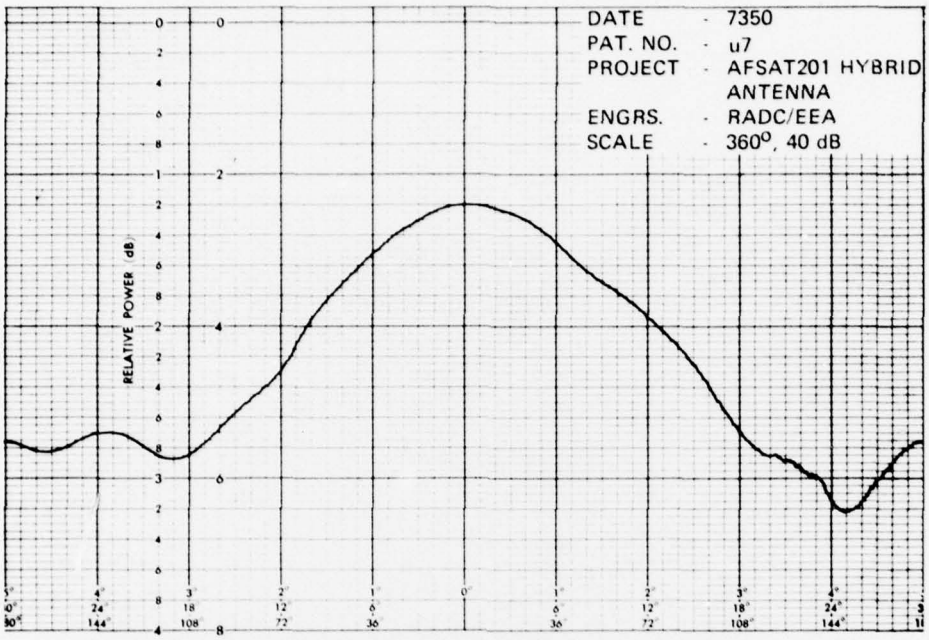

Figure 66. UHF Radiation Pattern With Grid Reflector (E-Plane, 320 MHz)

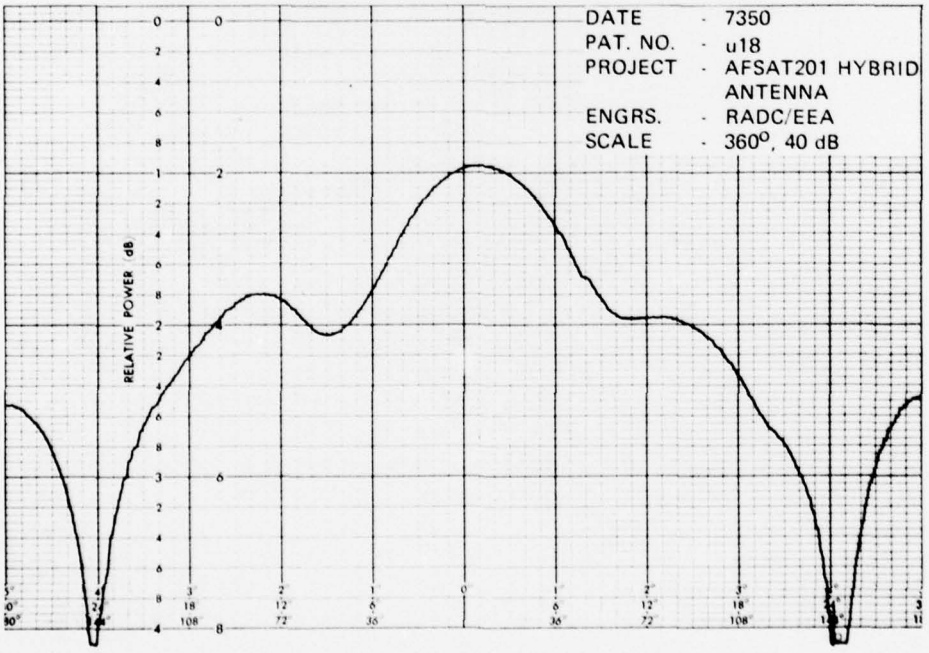

Figure 67. UHF Radiation Pattern With Grid Reflector (H-Plane, 320 MHz)

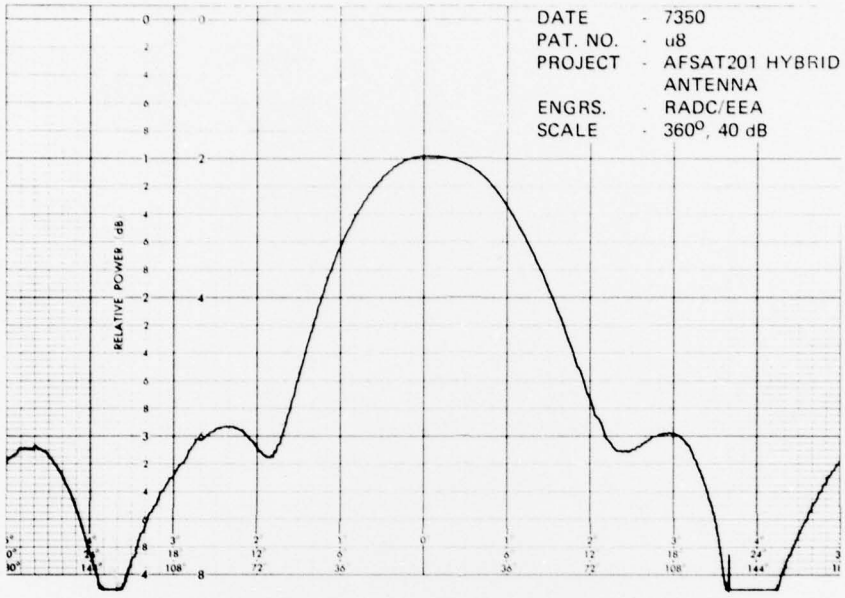

Figure 68. UHF Radiation Pattern With Grid Reflector (E-Plane, 340 MHz)

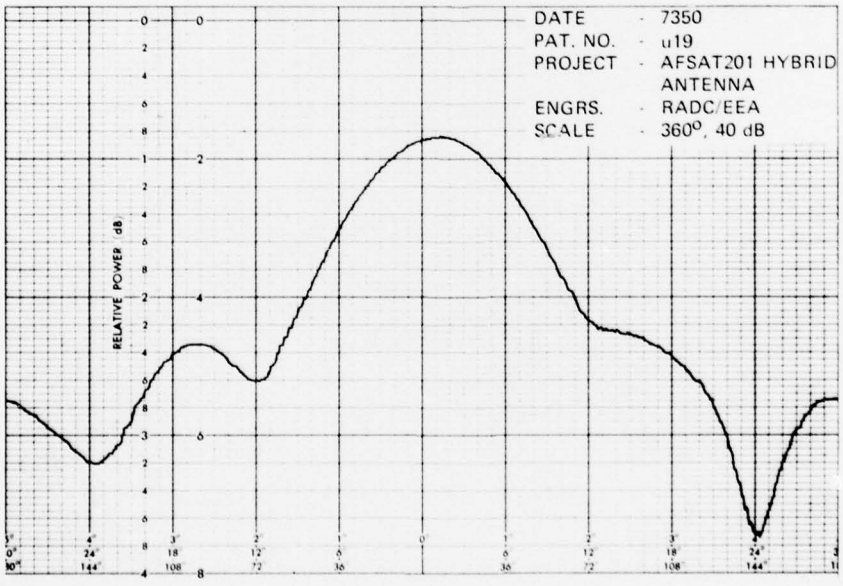

Figure 69. UHF Radiation Pattern With Grid Reflector (H-Plane, 340 MHz)

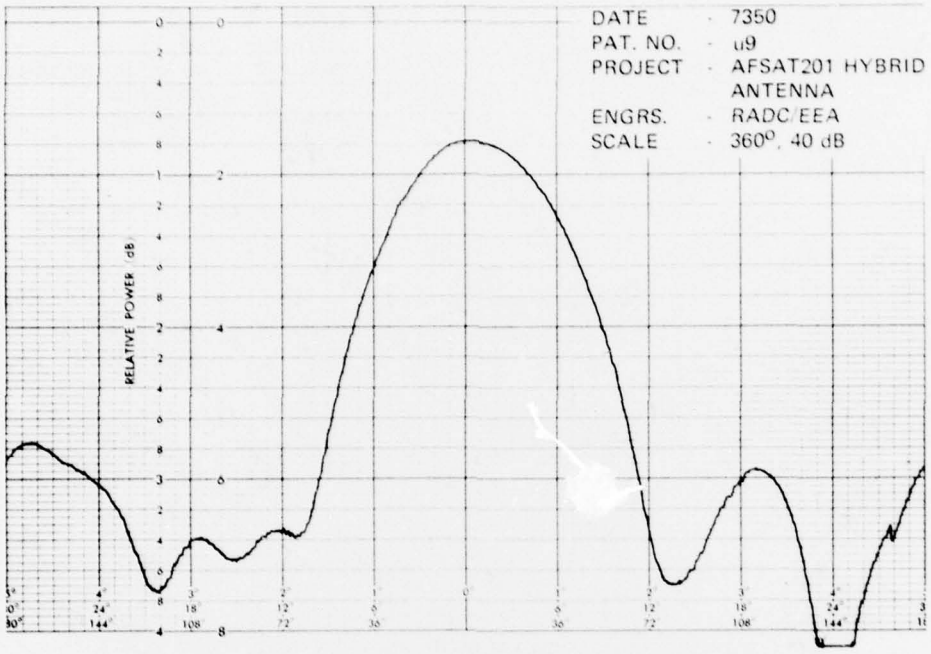

Figure 70. UHF Radiation Pattern With Grid Reflector (E-Plane, 360 MHz)

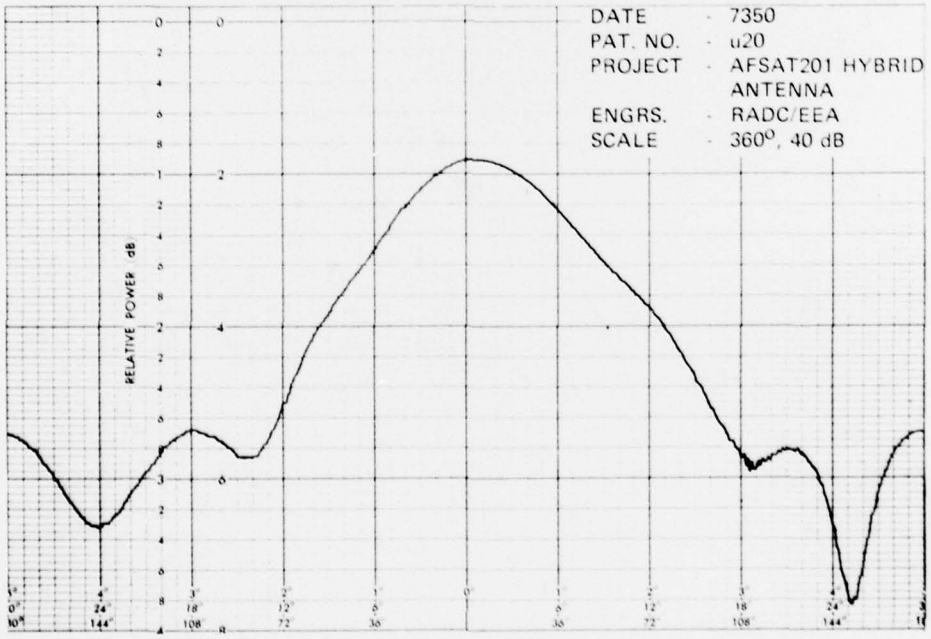

Figure 71. UHF Radiation Pattern With Grid Reflector (H-Plane, 360 MHz)

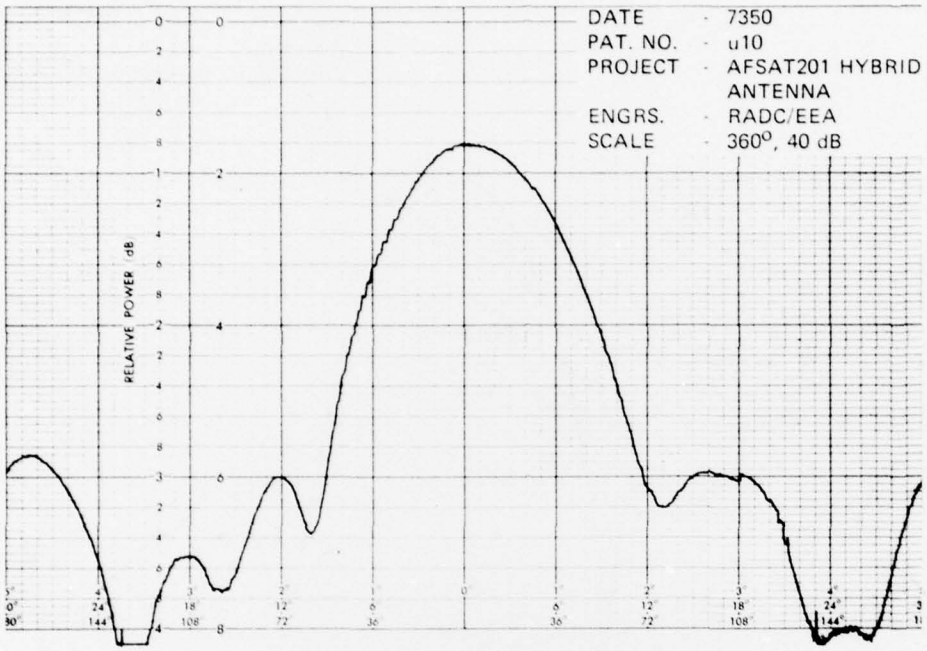

Figure 72. UHF Radiation Pattern With Grid Reflector (E-Plane, 380 MHz)

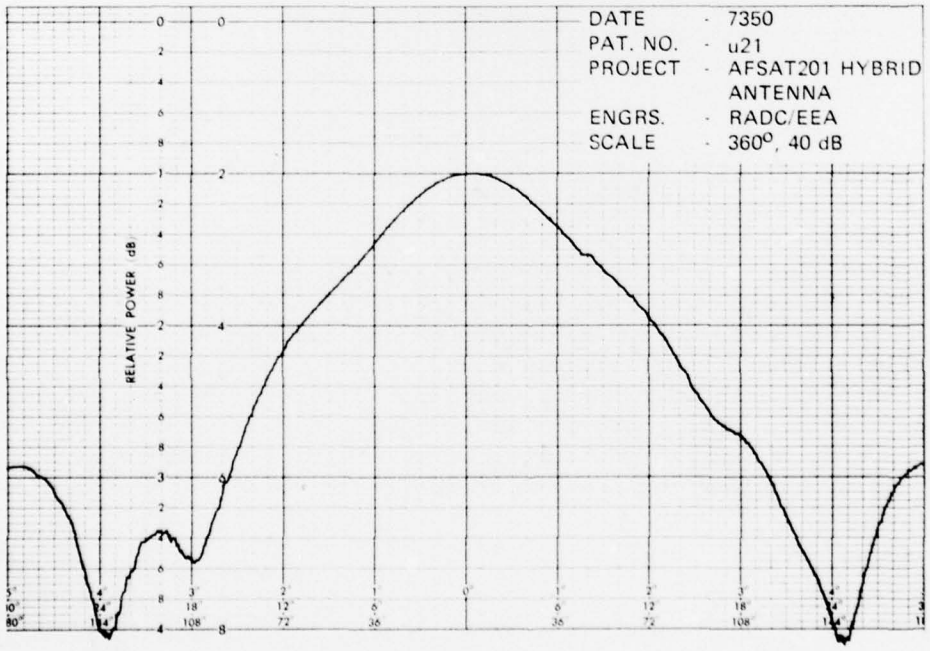

Figure 73. UHF Radiation Pattern With Grid Reflector (H-Plane, 380 MHz)

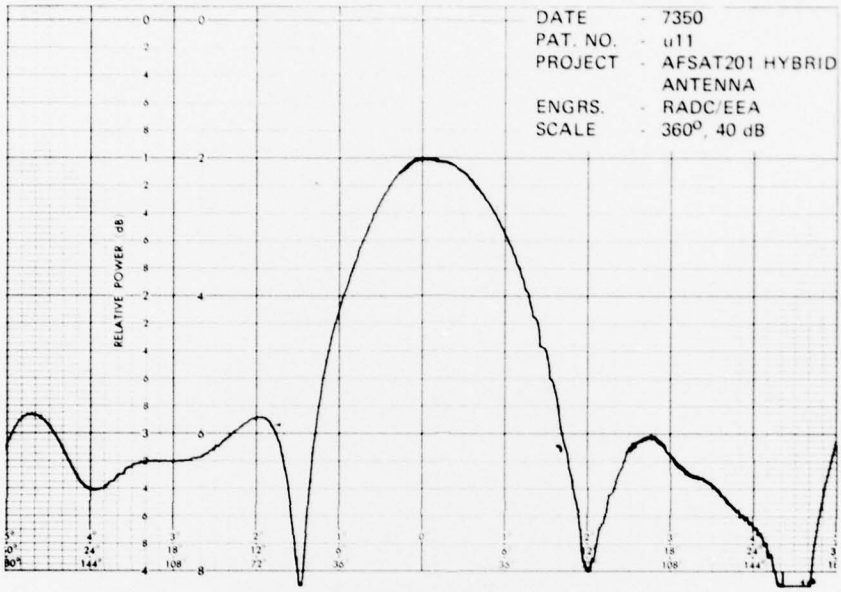

Figure 74. UHF Radiation Pattern With Grid Reflector (E-Plane, 400 MHz)

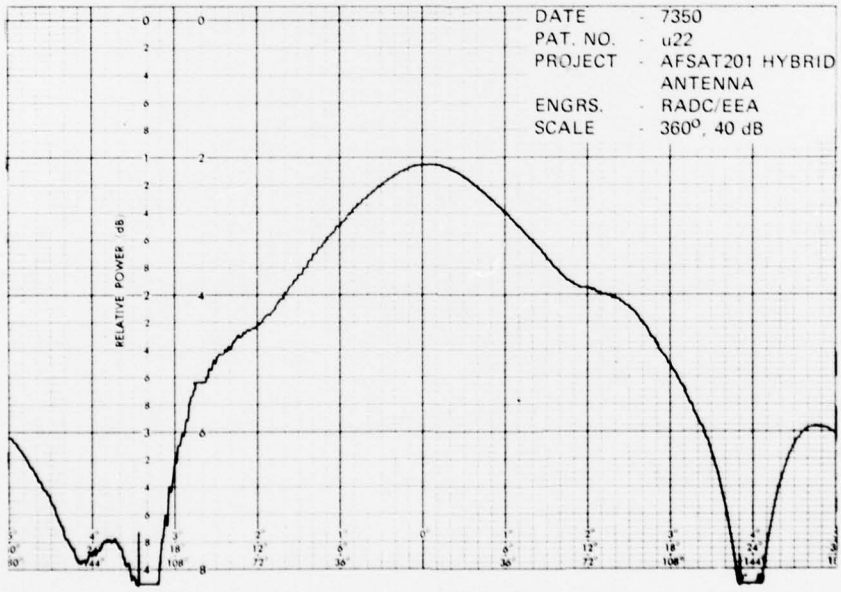

Figure 75. UHF Radiation Pattern With Grid Reflector (H-Plane, 400 MHz)

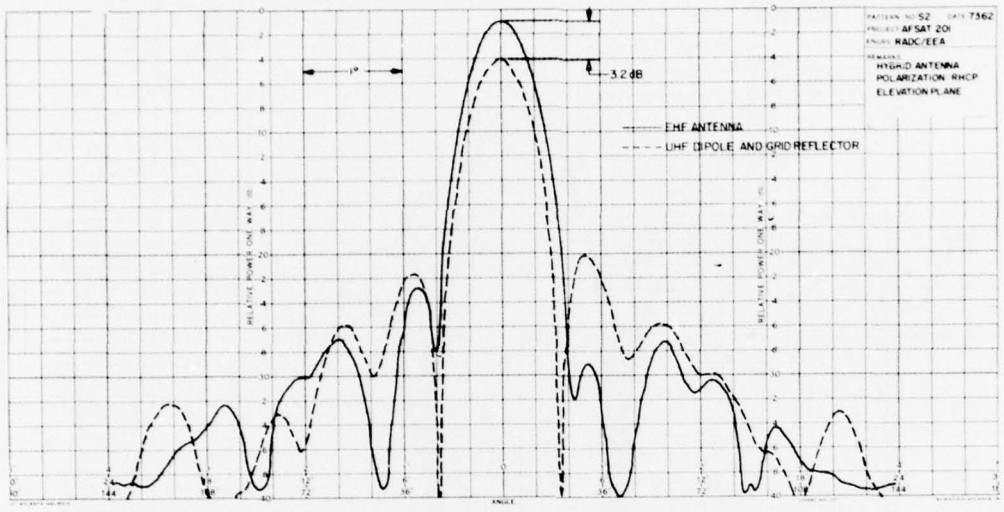

Figure 76. EHF Radiation Pattern With UHF Dipole and Grid Reflector (Elevation Plane)

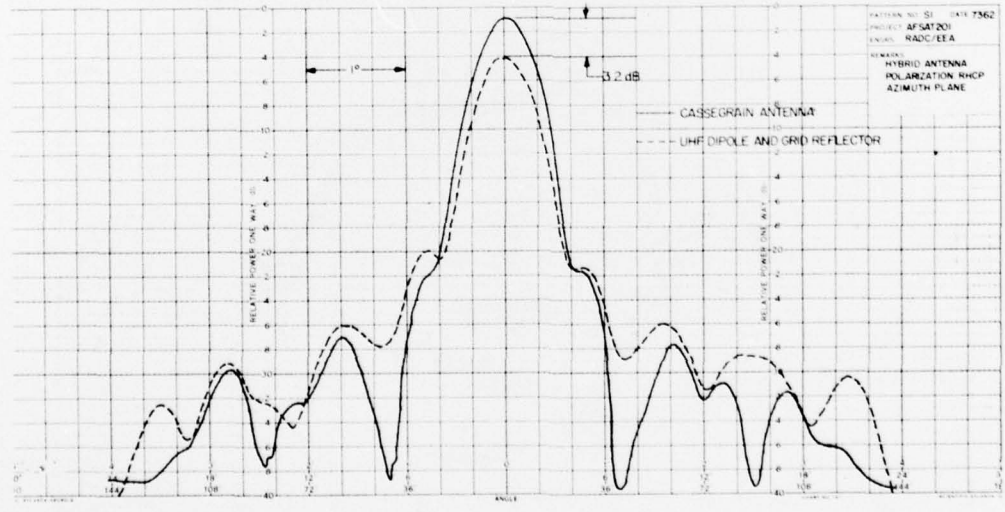

Figure 77. EHF Radiation Pattern With UHF Dipole and Grid Reflector (Azimuth Plane)

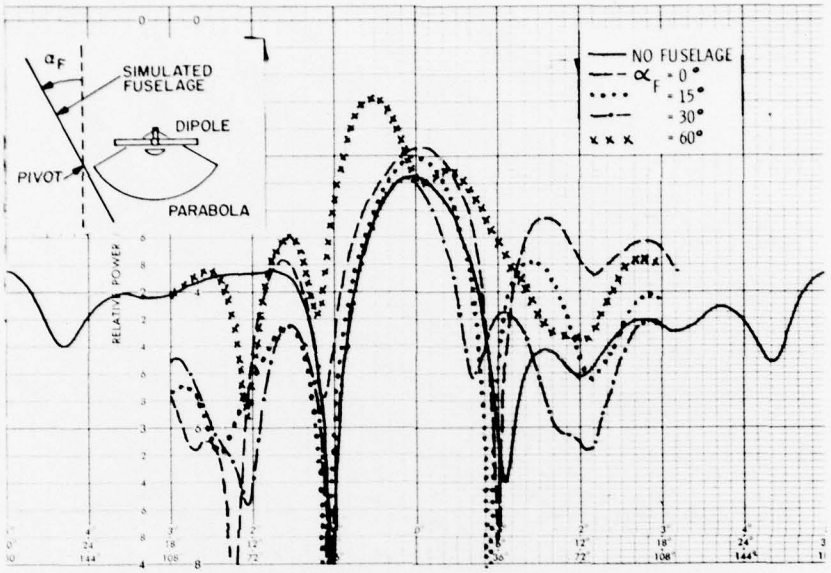

Figure 78. UHF Radiation Patterns With Fuselage Interference (E-Plane, 300 MHz)

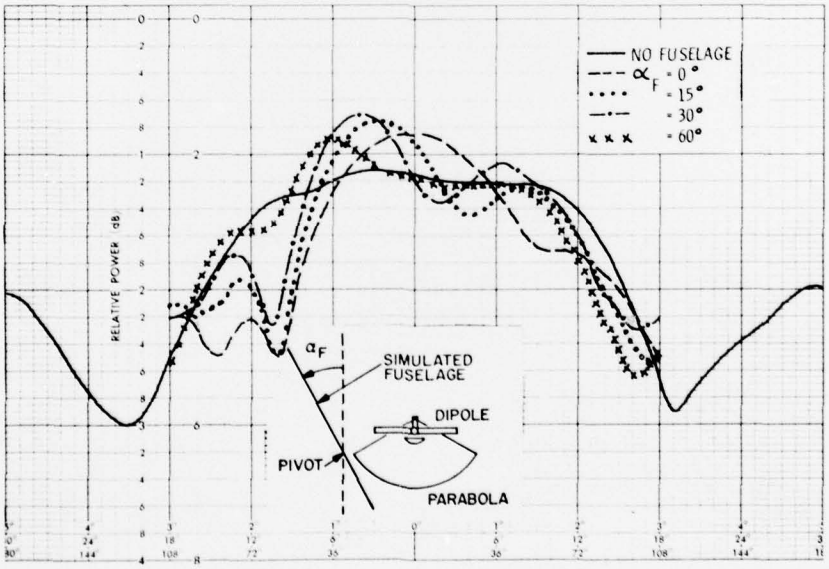

Figure 79. UHF Radiation Patterns With Fuselage Interference (H-Plane, 300 MHz)

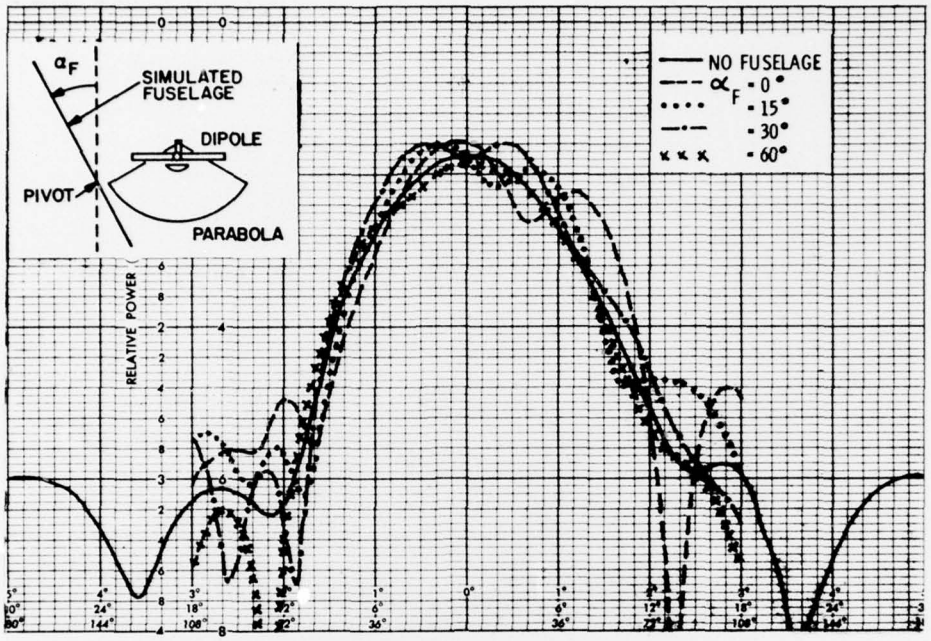

Figure 80. UHF Radiation Patterns With Fuselage Interference (E-Plane, 340 MHz)

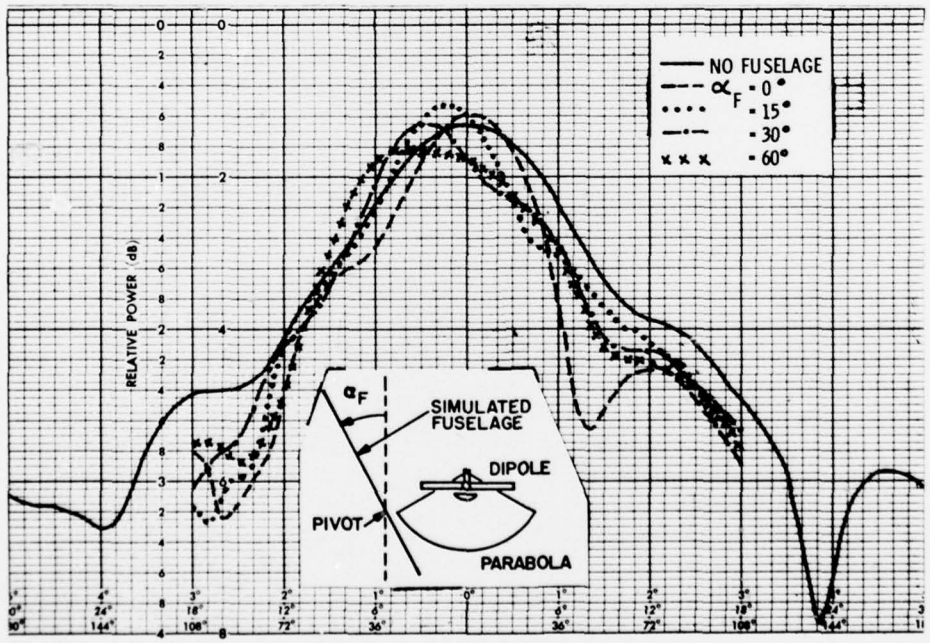

Figure 81. UHF Radiation Patterns With Fuselage Interference (H-Plane, 340 MHz)

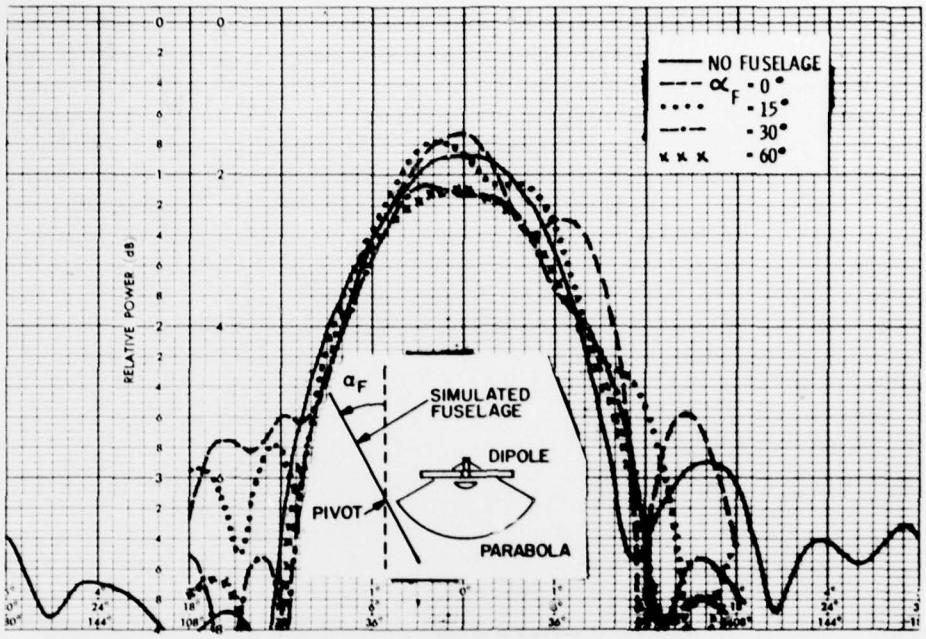

Figure 82. UHF Radiation Patterns With Fuselage Interference (E-Plane, 380 MHz)

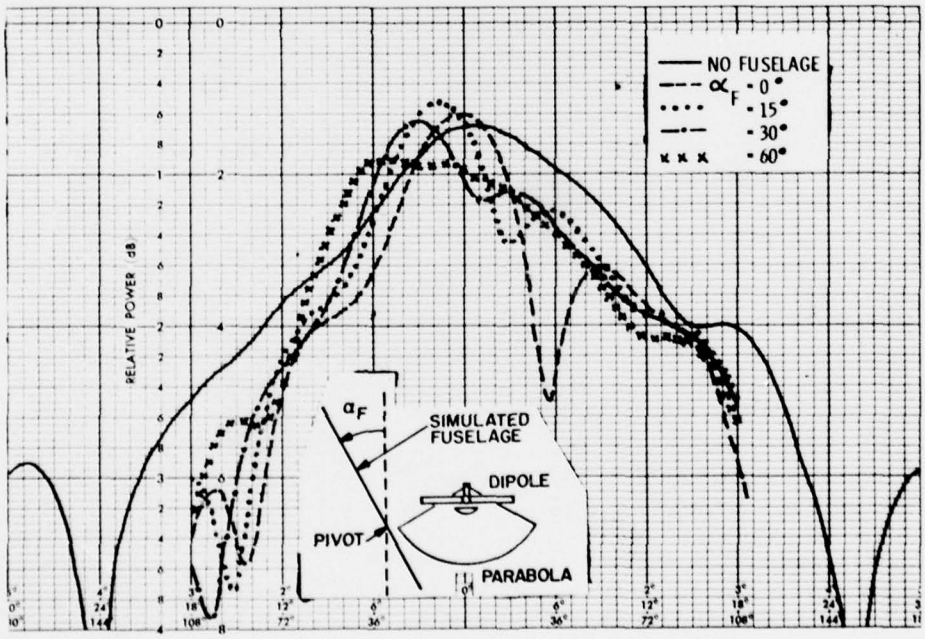

Figure 83. UHF Radiation Patterns With Fuselage Interference (H-Plane, 380 MHz)